RESEARCH ARTICLE

Heterogeneity and ontogeny of mouse thymic macrophages reveal a requirement for *Csf1r*-expressing myeloid cells during early T cell development

Helen Wang[1,2†], Vinothkumar Rajan[1,2†], Anthony Wong[1,3], Slava Epelman[1,3,4,5], Juan Carlos Zúñiga-Pflücker[1,2*]

[1]Department of Immunology, University of Toronto, Toronto, Canada; [2]Biological Sciences, Sunnybrook Research Institute, Toronto, Canada; [3]Toronto General Hospital Research Institute, University Health Network, Toronto, Canada; [4]Ted Rogers Centre for Heart Research, Translational Biology and Engineering Program, Toronto, Canada; [5]Peter Munk Cardiac Centre, University Health Network, Toronto, Canada

eLife Assessment

This study characterises the heterogeneity and developmental origins of macrophages in the thymus and demonstrates a role for Csf1r-expressing myeloid cells in the first step of T cell development. The state-of-the-art experiments provide **convincing** evidence, and the assessors concerns were addressed in the revised submission. These results provide an **important** advance that furthers our understanding of thymus biology, especially in view of the contribution of heterogenous thymic macrophage subpopulations.

***For correspondence:** jczp@sri.utoronto.ca

[†]These authors contributed equally to this work.

Competing interest: See page 22

Funding: See page 22

Preprint posted
01 September 2025
Sent for Review
09 April 2026
Reviewed preprint v1
22 June 2026
Reviewed preprint v2
21 September 2026
Version of Record
07 October 2026

Reviewing Editor: Sarah Russell, Peter MacCallum Cancer Centre, Australia

© Copyright Wang, Rajan *et al*. This article is distributed under the terms of the Creative Commons Attribution License, which permits unrestricted use and redistribution provided that the original author and source are credited.

Abstract Thymic macrophages (TMs) maintain tissue homeostasis by clearing the large numbers of apoptotic cells generated during T cell development, but how TM heterogeneity relates to their developmental origin and role in thymocyte maturation remains incompletely understood. Using complementary flow-cytometric, single-cell transcriptomic, and genetic approaches, we resolved two major TM populations corresponding to TIMD4$^+$ cortical and CX3CR1$^+$ medullary/cortico-medullary macrophages. TIMD4$^+$ VCAM1$^+$ TMs displayed a prominent efferocytosis and apoptotic-cell-clearance program, whereas TIMD4$^-$ VCAM1$^+$ TMs were enriched for antigen-presentation and interferon-response pathways. Fate mapping revealed unequal progenitor contributions to these populations, and CCR2 deficiency selectively reduced TIMD4$^-$ VCAM1$^+$ TMs, and thymic monocytes, supporting ongoing input from circulating precursors. Exploratory pseudotime analysis further identified a transcriptional continuum from *Ly6c2*$^+$*Ccr2*$^+$ monocytes toward macrophage states. Using MaFIA fetal thymic organ cultures, AP20187-mediated depletion of *Csf1r*-expressing myeloid cells reduced CD4$^+$CD8$^+$ thymocyte differentiation and produced a coordinated accumulation of DN3 cells, loss of DN4 cells, and reduction in CD27 expression. These convergent changes identify the DN3-to-DN4 transition as a developmental stage that requires an intact *Csf1r*-expressing myeloid compartment and establish a functional connection between the thymic myeloid niche and early αβ T cell development. Together, our study refines the phenotypic and developmental organization of mouse TMs and reveals a previously underappreciated requirement for myeloid-cell support during progression through the β-selection checkpoint.

Introduction

The thymus is the primary lymphoid organ dedicated to the generation of a diverse and self-tolerant repertoire of T lymphocytes, a process fundamental to adaptive immunity (**Miller, 2011**). This intricate T cell developmental program unfolds within a highly organized microenvironment composed of thymic epithelial cells (TECs), endothelial cells, and various hematopoietic populations, which collectively provide the essential signals for thymocyte differentiation, proliferation, and selection (**Shah and Zúñiga-Pflücker, 2014**; **James et al., 2021**; **Petrie and Zúñiga-Pflücker, 2007**). The developmental journey of a T cell begins when bone marrow-derived thymic seeding progenitors (TSPs) enter the thymus at the cortico-medullary junction (CMJ) and commit to the T cell lineage, initiating a multistage differentiation cascade (**Foss et al., 2001**; **Goldschneider et al., 1986**; **Benz et al., 2008**).

This journey is punctuated by a series of stringent checkpoints that assess the integrity and functionality of the nascent T cell receptor (TCR) repertoire (**Ciofani and Zúñiga-Pflücker, 2010**; **Moran and Hogquist, 2012**). The earliest stages occur in the thymic cortex, where progenitors, lacking expression of CD4 and CD8, termed double-negative (DN) thymocytes (**Goldschneider et al., 1986**), start to differentiate, which is characterized by the expression of CD44 and CD25 (**James et al., 2021**; **Petrie and Zúñiga-Pflücker, 2007**). Progression from the DN1 ($CD44^+CD25^-$) to the DN2 ($CD44^+CD25^+$) and DN3 ($CD44^-CD25^+$) stages is marked by the initiation of V(D)J recombination at the *Tcrb*, *Tcrg*, and *Tcrd* gene loci (**Miller, 2011**). The DN3 stage represents the first critical checkpoint in αβ T cell development, known as β-selection (**Michie and Zúñiga-Pflücker, 2002**; **Das et al., 2016**). Here, thymocytes that have successfully rearranged a functional TCRβ chain pair it with the invariant pre-TCRα chain (pTα) to form the pre-TCR complex. Successful signaling through this complex provides vital survival, proliferation, and differentiation cues, allowing the cell to progress to the DN4 stage and subsequently to the $CD4^+CD8^+$ double-positive (DP) stage (**Falk et al., 2001**; **Rothenberg et al., 2008**). Thymocytes failing to generate a functional pre-TCR are eliminated via apoptosis, ensuring that only cells with a viable TCRβ chain continue their developmental progression (**Falk et al., 2001**).

Following β-selection, DP thymocytes undergo further TCRα chain rearrangement and are subjected to two additional selection events. Positive selection ensures that the fully assembled αβ TCR can recognize self-peptides presented by major histocompatibility complex (MHC) molecules on cortical (c)TECs, a process essential for TCR MHC-restriction (**Klein and Petrozziello, 2025**; **Janeway et al., 2001**; **Murata et al., 2008**). Subsequently, negative selection in the medulla eliminates thymocytes whose TCRs bind with high affinity to self-peptides presented by medullary (m)TECs and dendritic cells (DCs), thereby establishing central tolerance (**Gotter et al., 2004**; **Proietto et al., 2008**). These selection processes are notably stringent, resulting in the apoptotic death of over 95% of all developing thymocytes (**Palmer, 2003**).

Integral to this journey and processes are thymic macrophages (TMs), which have long been recognized for their critical homeostatic function. Residing in both the cortex and medulla, TMs are exceptionally efficient phagocytes, responsible for the swift and silent clearance of the millions of apoptotic thymocytes generated daily (**Klein et al., 2014**; **Hanna et al., 2011**; **Baratin et al., 2017**; **Wang and Zúñiga-Pflücker, 2022**). This process, known as efferocytosis, is vital for preventing the release of potentially immunogenic and inflammatory intracellular contents and maintaining the integrity of the thymic architecture (**Italiani and Boraschi, 2014**). However, this view of TMs as mere 'housekeepers' is rapidly evolving. Recent advances, particularly single-cell RNA sequencing (scRNA-seq), have revealed significant heterogeneity within the TM compartment, suggesting functional specialization (**Zhou et al., 2022**). Two principal subsets have been identified in the adult mouse thymus: cortical TIMD4 +macrophages, which have potent efferocytosis function, and CX3CR1+macrophages, which are enriched at the CMJ and express genes associated with antigen presentation, suggesting a potential role in negative selection (**Zhou et al., 2022**).

Recent work by Zhou et al. established that adult mouse TMs comprise embryonically derived TIMD4 +macrophages localized predominantly in the cortex and adult hematopoietic stem-cell-derived CX3CR1+macrophages enriched in the medulla and CMJ (**Zhou et al., 2022**). These findings provided an important framework for TM heterogeneity and ontogeny. However, the surface-marker relationships that permit prospective resolution of these populations, the requirements that maintain them, and their contribution to early thymocyte development remain incompletely defined. In particular, β-selection is commonly viewed as a thymocyte-intrinsic checkpoint, even though DN3-to-DN4 progression occurs within a multicellular thymic microenvironment. This raises the possibility

that resident myeloid cells provide supportive functions that help developing thymocytes successfully navigate this transition.

Here, we combined high-parameter flow cytometry, single-cell RNA sequencing, genetic fate mapping, CCR2 and SpiC deficiency, and fetal thymic organ culture (FTOC) to define the phenotypic organization, developmental contributions, and functional significance of the thymic myeloid compartment. Our results identify VCAM1 as a useful component of a prospective gating strategy for the two major TM populations, demonstrate CCR2 dependence of the TIMD4- VCAM1 +population, and reveal that depletion of *Csf1r*-expressing myeloid cells compromises thymocyte progression across the DN3-to-DN4 checkpoint.

Results

Identification of two distinct tissue-resident macrophage subsets in the adult thymus

To investigate the heterogeneity of phagocytic cells within the thymus, we performed multi-parameter flow cytometry on hematopoietic cells ($CD45^+$) from the thymus of adult mice. We first identified the total TM population based on the co-expression of the canonical markers CD64 and F4/80 (***Figure 1A and B***). The majority of these $CD64^+$ $F4/80^+$ cells also expressed the phagocytic receptor MerTK, consistent with their identity as macrophages (***Thorp et al., 2008***).

Analysis of TIMD4 and VCAM1 expression resolved three populations within the CD64 +F4/80+gate: a major TIMD4 +VCAM1+population, a smaller TIMD4- VCAM1 +population, and a minor TIMD4- VCAM1- population (***Figure 1C–E***). The two VCAM1 +gates correspond phenotypically to the TIMD4 +cortical and TIMD4-/CX3CR1+medullary/cortico-medullary macrophage populations described by Zhou et al. while VCAM1 provides an additional prospective discriminator (***Zhou et al., 2022***). Both VCAM1 +populations expressed the macrophage-associated $Mafb^{mCherry}$ reporter. By contrast, the TIMD4- VCAM1- population was *Mafb*-low/negative and displayed high $Csf1r^{EGFP}$, consistent with a monocyte-enriched phenotype (***Figure 1F***). These results establish a flow-cytometric framework that links our prospectively defined populations to the major TM states identified transcriptionally and anatomically in prior work (***Zhou et al., 2022***).

Short-term intravenous (i.v.) labeling with anti-CD45 demonstrated that most TIMD4 +VCAM1+and TIMD4- VCAM1 + cells were shielded from the circulation, supporting their predominantly parenchymal localization (***Figure 2A–C***). The broad Ly6C+CD11b+ comparison gate contained both iv-labeled and unlabeled cells, whereas the more stringently defined TIMD4- VCAM1- gate within CD64 +F4/80 + cells contained a smaller i.v.-labeled fraction. The two VCAM1 +populations were Ly6C-low/negative and expressed substantially less CCR2 than TIMD4- VCAM1- cells. CX3CR1 expression was enriched in the TIMD4- VCAM1 +population relative to TIMD4 +VCAM1+macrophages (***Figure 2D and E***), further aligning these populations with the TIMD4 +and CX3CR1+TM states described previously (***Zhou et al., 2022***). In contrast, the TIMD4- VCAM1- population was enriched for Ly6C, CCR2, and CX3CR1, supporting its designation as a monocyte-enriched thymic population.

Together, these data identify two predominantly parenchymal VCAM1 +TM populations and distinguish them from a TIMD4- VCAM1- monocyte-enriched population. This gating framework connects surface phenotype, anatomical accessibility, and reporter expression, enabling prospective analysis of the major TM populations.

Transcriptomic profiling by scRNA-seq confirms two functionally distinct macrophage subsets

To gain deeper insight into the transcriptional identities of these macrophage populations, we performed scRNA-seq on sorted thymic CD45 +CD64 + cells. Unbiased clustering of the resulting 3153 cells revealed five distinct myeloid clusters, including monocytes, proliferating macrophages, and two major quiescent macrophage populations that corresponded to our flow-cytometric gates (***Figure 3A***).

One major macrophage cluster expressed *Timd4*, *Vcam1*, *Mertk*, and *Maf*, corresponding to the TIMD4 +VCAM1+population (***Figure 3B***). A second cluster expressed *Vcam1* and *Cx3cr1*, aligning with the TIMD4- VCAM1 +population (***Table 1***). The TIMD4 +VCAM1+cluster also expressed *Spic*, the lineage-defining transcription factor required for splenic red pulp macrophages (RPMs) (***Kohyama***

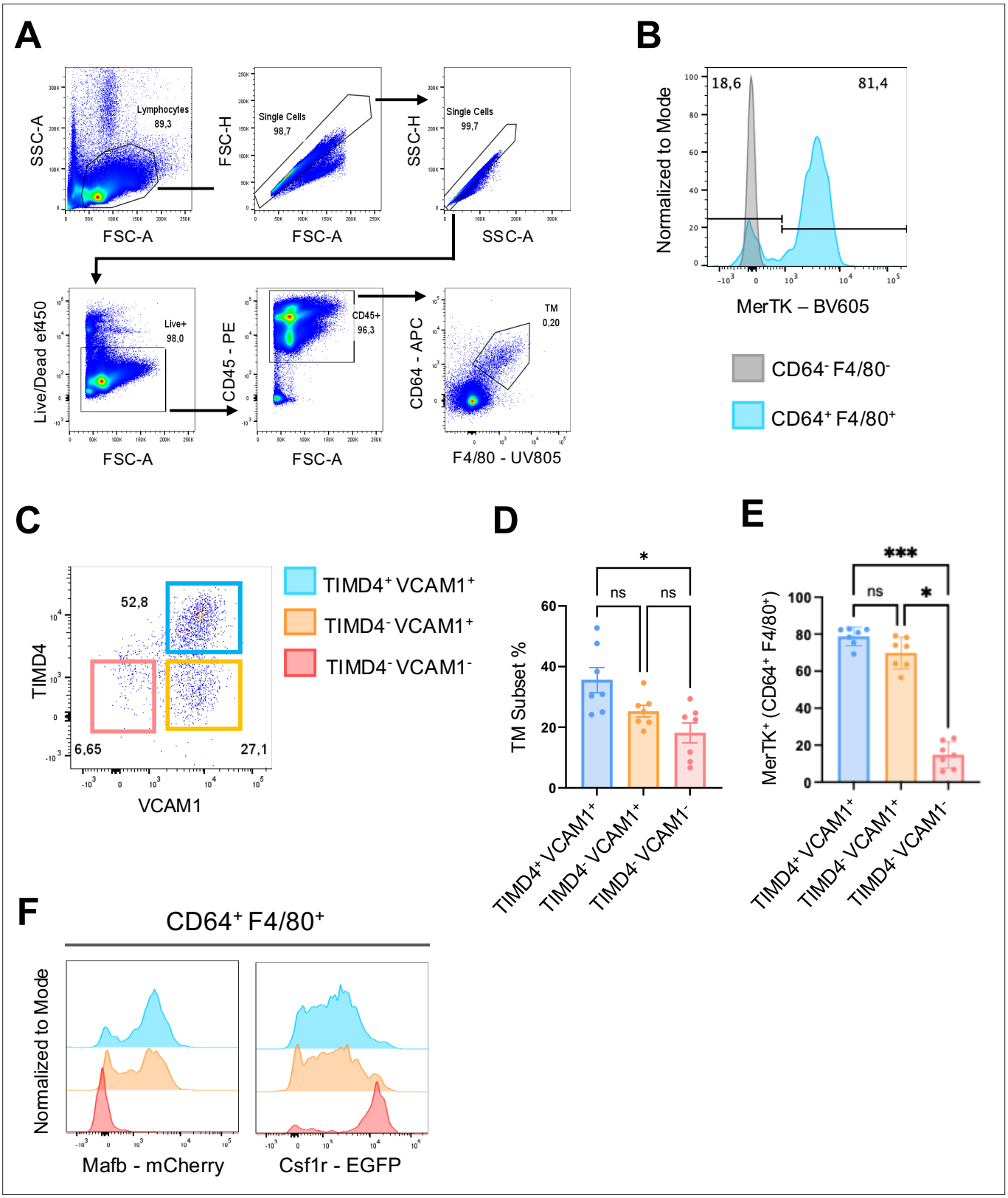


Figure 1. Flow-cytometric characterization of thymic macrophage populations. Thymuses from adult C57BL/6 mice were enzymatically digested and analyzed by flow cytometry. (**A**) Gating strategy for CD64+F4/80+TMs. (**B**) Representative MerTK histogram for TMs (blue) and CD64- F4/80- lymphocytes (red). (**C**) TIMD4/VCAM1 definition of TIMD4+VCAM1+, TIMD4- VCAM1+, and TIMD4- VCAM1- populations. (**D**) Frequencies of the three TM populations. (**E**) MerTK +frequencies. (**F**) *Mafb*^{mCherry} and *Csf1r*^{EGFP} reporter expression evaluated within the same TIMD4/VCAM1 gates defined in panel C. Data are mean ± SEM (n=7 per group from two independent experiments). Kruskal-Wallis test (*p≤0.05).

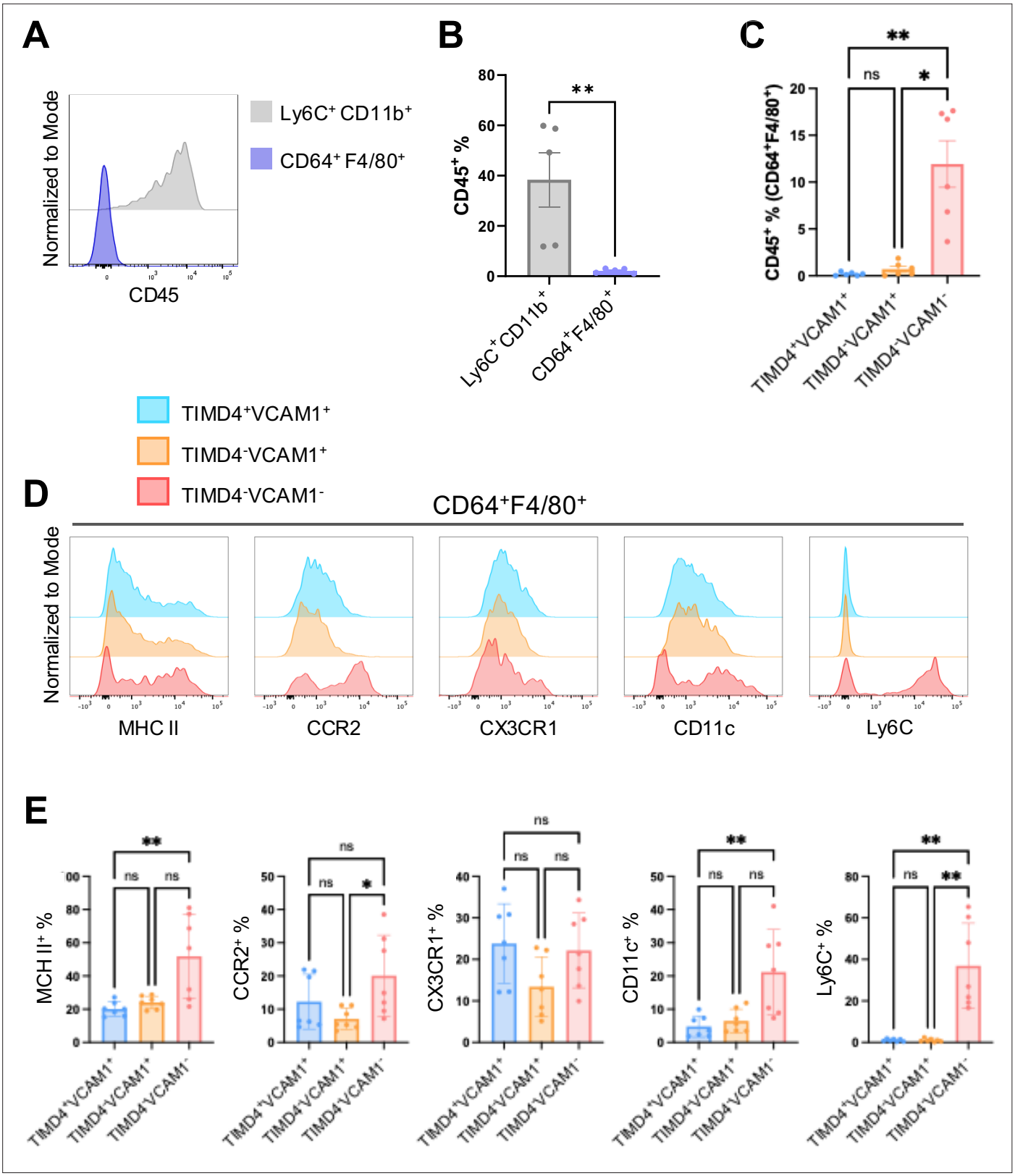


Figure 2. Intravascular labeling and monocyte-associated marker expression distinguish thymic myeloid populations. (**A**) Short-term intravenous (i.v.) anti-CD45 labeling identifies blood-exposed cells. (**B**) Frequencies of i.v. CD45-labeled cells in the broad Ly6C+CD11b+gate and the CD64+F4/80+macrophage gate. The Ly6C+CD11b+gate contains heterogeneous blood-exposed and parenchymal cells and is not equivalent to the TIMD4- VCAM1- gate. (**C**) i.v. CD45 labeling within TIMD4/VCAM1-defined populations. (**D, E**) Relative Ly6C, CCR2, and CX3CR1 signal across the three

Figure 2 continued on next page

Figure 2 continued

populations; descriptions are comparative rather than categorical. Data are mean ± SEM (n=5–7 per group from two independent experiments). Mann-Whitney test for two-group comparisons and Kruskal-Wallis test for three-group comparisons (*p≤0.05; **p≤0.01).

et al., 2009). We therefore examined the TM compartment in *Spic-/-* mice. As expected, splenic RPMs were markedly reduced, whereas total CD64 +F4/80+TM abundance was preserved (***Figure 3C***). Thus, despite sharing *Spic* expression with RPMs, maintenance of the overall TM compartment follows a distinct developmental program that does not require SpiC.

GO analysis revealed pronounced functional specialization between the two TM populations. TIMD4- VCAM1 +CX3CR1+TMs were enriched for antigen processing and presentation via MHC class I and for interferon-response pathways, consistent with a potential role in immune surveillance and T cell education (***Figure 4A***). Conversely, TIMD4 +VCAM1+TMs were strongly enriched for phagocytosis and endocytosis pathways, supporting specialization for efferocytic clearance of apoptotic thymocytes (***Figure 4B***). Individual genes contributing to these subset signatures, including H2-K1, H2-D1, and Runx3, are reported in ***Table 1***.

A subcluster within the TIMD4 +VCAM1+population co-expressed macrophage genes together with thymocyte-associated transcripts, including *Cd3g* and *Trac* (***Figure 3B***). In the context of the strong phagocytosis and endocytosis program in this population, the presence of thymocyte-derived transcripts is consistent with ongoing uptake of thymocyte material and provides additional support for efferocytic specialization. As with other phagocyte single-cell datasets, contributions from ambient RNA or rare multiplets cannot be fully distinguished from engulfed RNA, and we therefore interpret this signature together with the broader pathway evidence.

Exploratory Monocle3 analysis, rooted in *Ly6c2+Ccr2*+monocytes, placed monocytes and macrophage states along a connected transcriptional manifold. The ordering was consistent with progressive acquisition of macrophage-associated programs from a monocyte-like state and provided a transcriptional complement to the fate-mapping and CCR2-dependence experiments. As pseudotime models transcriptional relationships rather than prospective cell fate, it only allows us to predict a potential conversion between the two mature TM populations.

The thymic macrophage compartment undergoes dynamic remodeling during development

To understand how the TM compartment evolves in parallel with the thymus itself, we analyzed the number and composition of TM subsets during ontogeny, from embryonic development through adulthood. Consistent with known thymic biology, the absolute number of total thymocytes and TMs peaked in young, 3-week-old mice, before declining with age, indicating that the size of the TM pool is coupled to the overall cellularity of the organ (***Figure 5—figure supplement 1A and B***).

TM composition was extensively remodeled across development. At embryonic day 15 (E15), the thymic myeloid compartment was dominated by TIMD4- VCAM1- cells expressing CD11b and CCR2, consistent with recently recruited or immature myeloid precursors (***Figure 5A***). Following birth, TIMD4+VCAM1+macrophages expanded rapidly and became the dominant TM population during the period of maximal thymic growth (***Figure 5B***). With the onset of age-associated thymic involution, the proportion of TIMD4+VCAM1+macrophages declined, whereas TIMD4- VCAM1+macrophages progressively increased. These data reproduce the age-associated shift reported by Zhou et al. and show that our VCAM1-based gating strategy captures the developmental remodeling of the two major TM populations (***Zhou et al., 2022***).

Thus, the TM compartment is developmentally dynamic: immature myeloid cells predominate in the fetal organ, TIMD4+VCAM1+macrophages expand with postnatal thymic growth, and TIMD4-VCAM1+macrophages become increasingly prominent during involution. The changing abundance of these populations establishes the developmental context for their distinct ontogenetic contributions.

Thymic macrophage subsets arise from distinct developmental origins

Flt3^{Cre} × *Rosa26*^{mTmG} fate mapping revealed unequal developmental contributions to the two TM populations. In this model, cells with a history of FLT3 expression switch from membrane Tomato to membrane GFP, whereas FLT3-independent cells remain Tomato+ (***Figure 6A***; ***Epelman et al., 2014***). TIMD4+VCAM1+macrophages contained a large Tomato+fraction, demonstrating a substantial

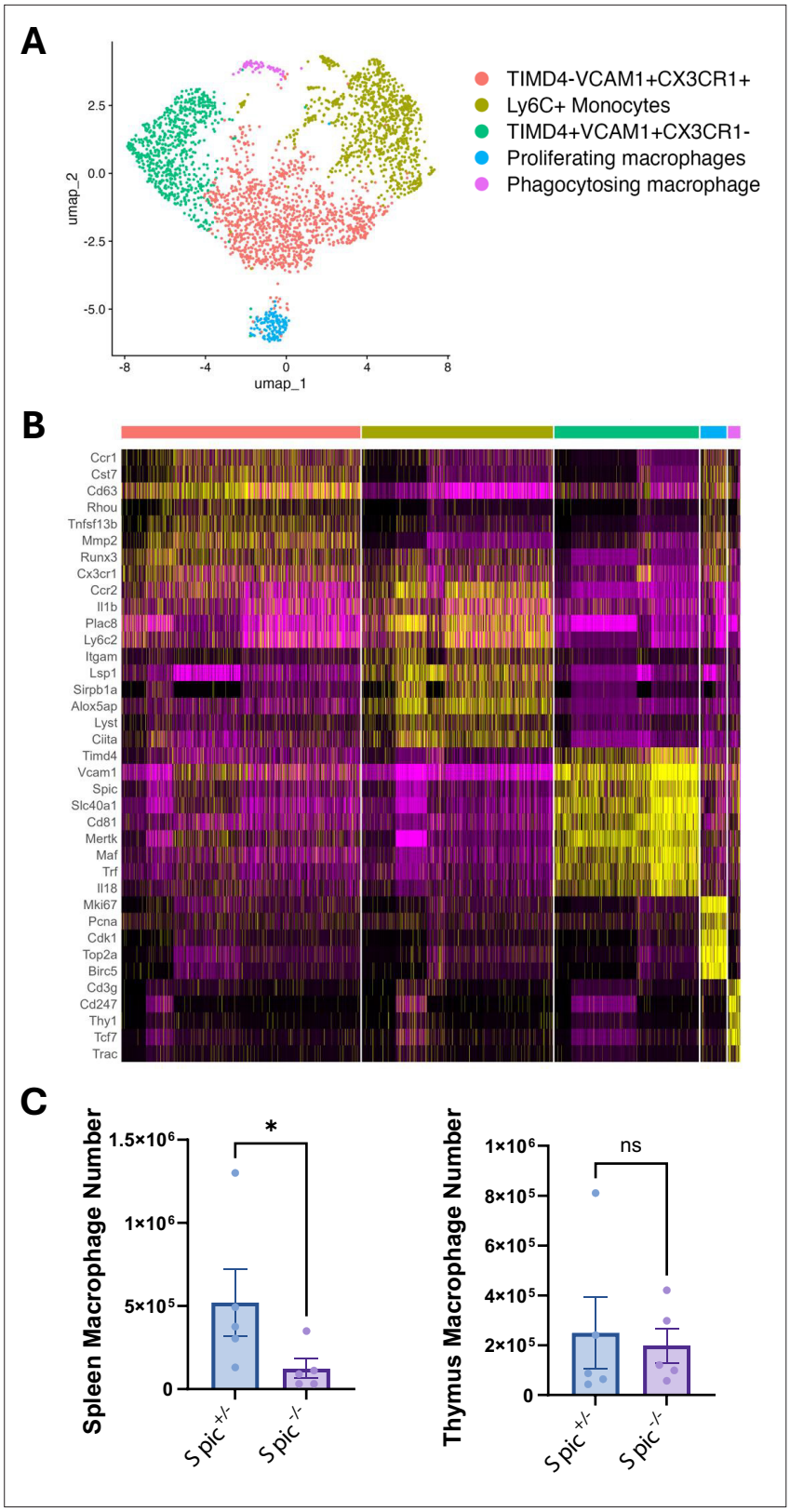


Figure 3. Single-cell transcriptomic profiles of thymic macrophages. CD64 + cells from six-week-old C57BL/6 thymuses were analyzed by 10 X Genomics 3' scRNA-seq in two independent experiments, each pooling six mice, and integrated with the Zhou et al. dataset using Harmony. (**A**) UMAP showing five annotated myeloid clusters; panel colors denote cluster identity. (**B**) Heatmap of row-scaled differentially expressed genes; yellow and purple

Figure 3 continued on next page

Figure 3 continued

represent higher and lower relative scaled expression, respectively, and are not equivalent to flow-cytometric fluorescence intensity. (**C**) Total CD64+F4/80+macrophage numbers in thymus and spleen of *Spic-/-* and control mice; TM subpopulations were not separately quantified in this panel. Data are mean ± SEM (n=4–5 per group from two independent experiments), Mann-Whitney test (*p≤0.05).

contribution from FLT3-independent embryonic/fetal precursors. In contrast, TIMD4- VCAM1+macrophages and thymic monocytes were predominantly GFP+, consistent with derivation from FLT3-expressing hematopoietic progenitors (***Figure 6B and C***). Tomato+GFP + events likely represent ongoing reporter transition or persistence of stable membrane Tomato after recombination and were included within the overall assessment of reporter history rather than treated as a separate lineage.

Because TIMD4- VCAM1+macrophages showed greater FLT3-lineage history than their TIMD4+VCAM1+counterparts, we asked whether maintenance of this population depends on CCR2-mediated precursor recruitment. We therefore analyzed thymic myeloid populations in *Ccr2* knockout (*Ccr2-/-*) mice. Overall thymocyte cellularity and the abundance of TIMD4+VCAM1+macrophages were preserved, whereas both TIMD4- VCAM1+macrophages and the TIMD4- VCAM1- monocyte-enriched population were significantly reduced (***Figure 7A–D***). This selective effect links CCR2-dependent recruitment to maintenance of the TIMD4- VCAM1+arm of the TM network.

Together, the fate-mapping and *Ccr2-/-* data support a dual-contribution model for the TM network. TIMD4+VCAM1+macrophages retain a prominent FLT3-independent embryonic/fetal contribution, whereas TIMD4- VCAM1+macrophages show greater FLT3 history and depend on CCR2-mediated recruitment. The selective reduction of TIMD4- VCAM1+macrophages and thymic monocytes in *Ccr2-/-* mice provides functional evidence that circulating precursors contribute to maintenance of this arm of the TM compartment.

Table 1. Differentially expressed genes (DEGs) from scRNA-seq analysis.
List of DEGs with an average $\log_2$ fold change >1 and an adjusted p-value <0.01, ordered by adjusted $\log_2$ fold change.

Ly6C⁺ monocytes		**TIMD4⁺ VCAM1⁺ CX3CR1⁻**		**TIMD4⁻ VCAM1⁺ CX3CR1⁺**	
Lsp1	*Ahnak*	*Cd163*	*Ccl2*	*Gpnmb*	*Lhfpl2*
Sirpb1a	*Cytip*	*Mrc1*	*Ccl4*	*Tnfsf13b*	*Chst2*
Gm34084	*Ifitm2*	*Mertk*	*Adgre1*	*Lhfpl2*	*Mmp2*
Alcam	*S100a11*	*Spic*	*Adgre2*	*Chst2*	*Pmepa1*
Cbfa2t3	*Ramp1*	*Timd4*	*Hmox1*	*Mmp2*	*Oas3*
Sirpb1b	*Lyst*	*Vcam1*	*Tlr7*	*Pmepa1*	*Cst7*
Cnn2	*Ccl6*	*Clec1b*	*Axl*	*Oasl1*	*Zmynd15*
Samsn1	*Itga4*	*Stab2*	*Fgr*	*Cst7*	*H2-Q7*
Itgam	*Il17ra*	*Fcgrt*	*Ccl8*	*Zmynd15*	*Ccr5*
Alox5ap	*Ccr2*	*Tgm2*	*Id2*	*H2-M2*	*H2-T22*
Emb	*Ly6c2*	*P2ry12*	*Sirpa*	*Sh3pxd2b*	*Bst2*
Traf1	*Il1b*	*Cd86*	*Runx1*	*Kctd14*	*Stat2*
Dpp4	*Batf3*	*Tlr4*	*Stat5b*	*Ifit1*	*Cebpa*
S100a10	*Rbpj*	*Il18*	*Cd84*	*Fam20c*	*Il1rn*
Plac8		*Ptgs1*	*Mapk14*	*Cp*	*Cxcl16*
Stap1		*Pparg*		*Spsb1*	
Sirpb1c		*Adamdec1*		*Gpnmb*	
Rnase6		*Cd38*		*Tnfsf13b*	

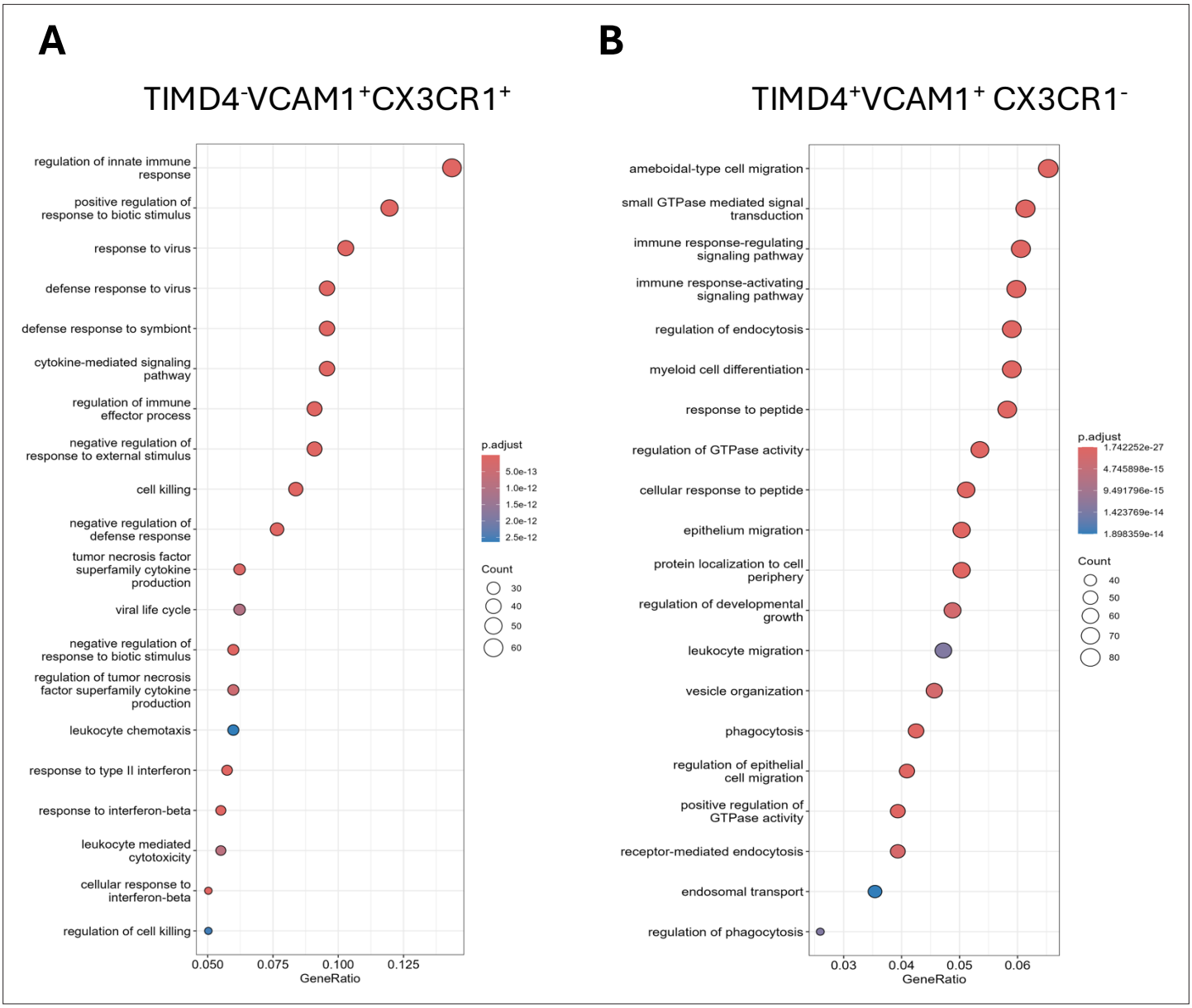


Figure 4. Gene Ontology pathway analysis of TM populations. (**A**) Top enriched pathways in TIMD4- VCAM1+CX3CR1+TMs. (**B**) Top enriched pathways in TIMD4+VCAM1+TMs. The panels display pathway-level enrichment; individual genes mentioned in the text are reported in ***Table 1*** and are not plotted separately in this Figure.

Csf1r-expressing myeloid cells support thymocyte progression across the DN3-to-DN4 checkpoint

To determine whether *Csf1r*-expressing myeloid cells contribute to early T cell development, we used the MaFIA (*Csf1r*-EGFP-NGFR/FKBP1A/TNFRSF6) model, in which AP20187 dimerizes an FKBP-Fas suicide protein and induces apoptosis in transgene-expressing cells (***Figure 8—figure supplement 1A and B***; ***Burnett et al., 2004***). Both TM populations and thymic monocytes expressed the *Csf1r*^{EGFP} reporter (***Figure 8—figure supplement 1C–E***), making this system well suited to perturb the thymic myeloid compartment. We applied this experimental approach to E15.5 fetal thymic organ culture (FTOC), which preserves the three-dimensional thymic microenvironment while avoiding systemic consequences of myeloid-cell depletion (***Jenkinson and Anderson, 1994***), and treated FTOCs from MaFIA mice with AP20187 at culture initiation (***Figure 8A***).

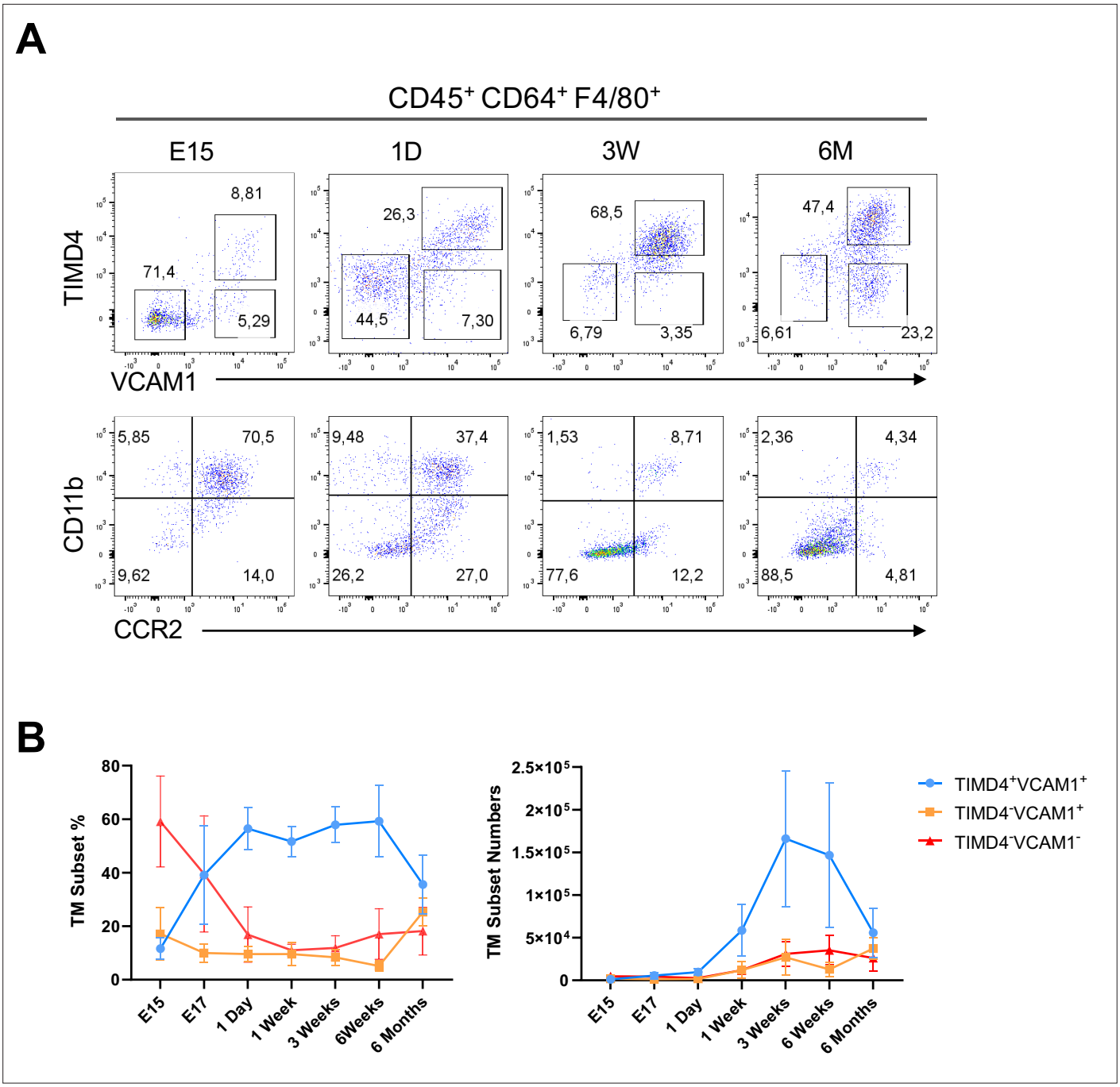


Figure 5. Developmental progression of TM subsets. Thymuses were harvested from mice at various developmental time points and enzymatically digested to prepare single-cell suspensions. Cells were stained with antibodies for flow cytometry analysis. (**A**) Expression of TM markers across different age groups. (**B**) Comparison of the numbers and percentages of TM in mice at different ages. Data are presented as mean ± SEM (n=4–12 per group from two to four independent experiments).

The online version of this article includes the following figure supplement(s) for figure 5:

Figure supplement 1. Changes in TM numbers during thymic development.

AP20187 treatment preserved the EpCAM +CD45- thymic epithelial-cell compartment (***Figure 8B***) while markedly reducing total TMs and both TIMD4/VCAM1-defined TM populations (***Figure 8E–H***). Importantly, TM abundance was unchanged in AP20187-treated C57BL/6 control FTOCs lacking the MaFIA transgene (***Figure 8F***), demonstrating that depletion required the transgenic suicide system rather than exposure to the dimerizer alone. Total thymocyte and CD11c+MHC-II^{high} DC numbers

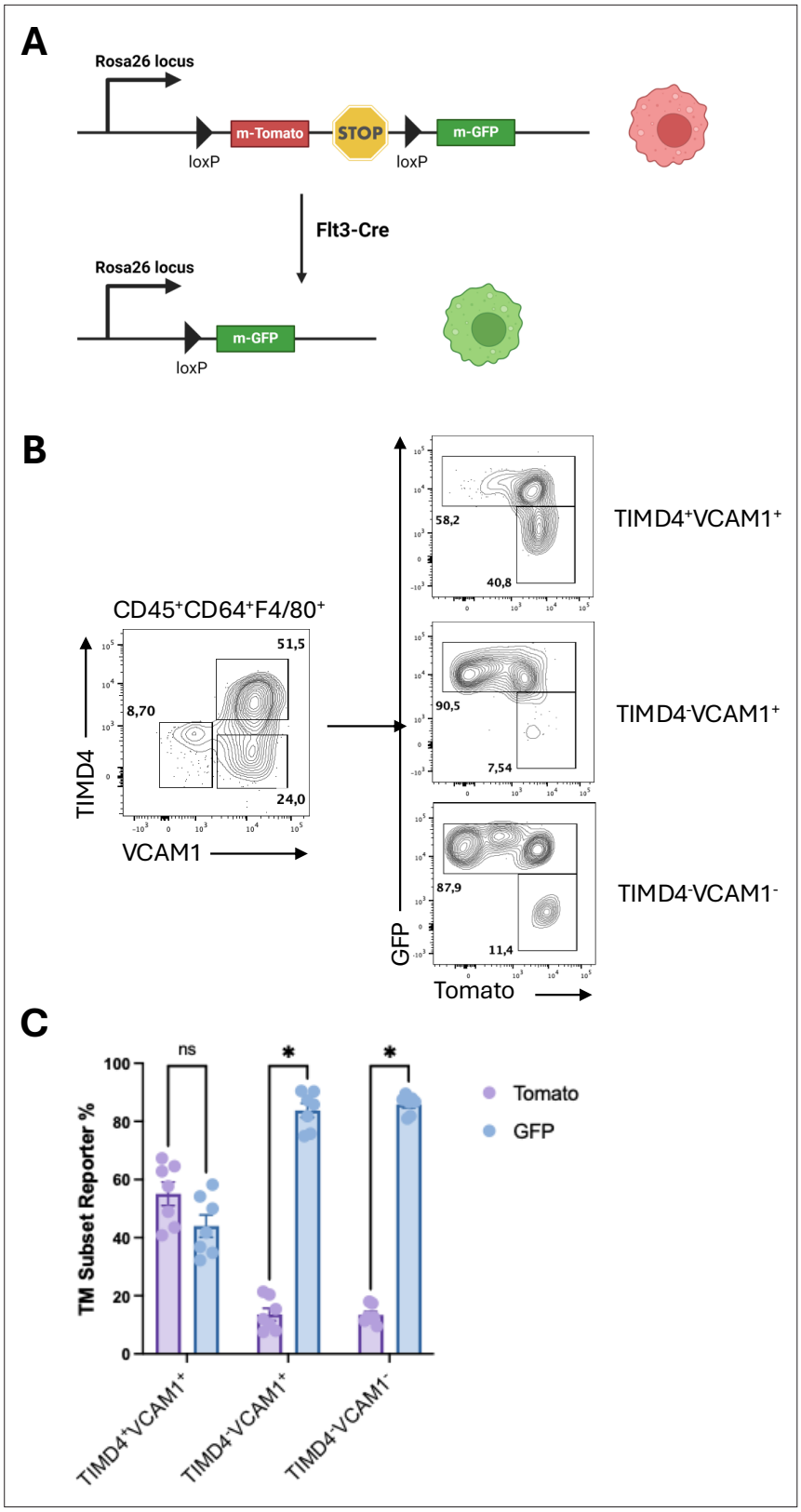


Figure 6. FLT3-Cre reporter history in thymic myeloid populations. (**A**) In *Flt3*^{Cre} × *Rosa26*^{mTmG} mice, Cre-mediated recombination switches membrane Tomato expression to membrane GFP in cells with *Flt3* expression history. (**B**) Representative Tomato/GFP profiles within TIMD4+VCAM1+, TIMD4- VCAM1+, and TIMD4- VCAM1- gates. Tomato +GFP + events are interpreted as reporter-transition/persistence events and not as a distinct lineage.

Figure 6 continued on next page

Figure 6 continued

(**C**) Reporter frequencies among the three populations. CX3CR1 phenotype is defined independently in ***Figure 2*** and is not displayed in this Figure. Data are mean ± SEM (n=7 per group from two independent experiments). Mann-Whitney tests with Holm-Šídák correction (***p≤0.001).

were also reduced (***Figure 8C and D***). These results establish efficient, transgene-dependent perturbation of the *Csf1r*-expressing thymic myeloid compartment within an epithelial environment that remained numerically intact.

Depletion of *Csf1r*-expressing cells impaired αβ T-lineage cell development, leading to a marked reduction in CD4 +CD8+double-positive (DP) thymocytes, whereas γδ T cell output was preserved (***Figure 9A–D***). To localize the αβ lineage developmental defect, we examined upstream DN populations (***Figure 10A***). AP20187-treated MaFIA FTOCs showed a coordinated accumulation of DN3 (CD44- CD25+) cells and reduction of DN4 (CD44- CD25-) cells (***Figure 10B***). The reciprocal change in sequential developmental populations identifies the DN3-to-DN4 transition as the principal stage affected by the loss of *Csf1r*-expressing cells.

We next examined CD27 expression, which is upregulated as DN3 thymocytes successfully receive pre-TCR-associated signals and progress through β-selection. The frequency of CD27 +DN3 cells was significantly reduced in AP20187-treated MaFIA FTOCs (***Figure 10C and D***). Considered together, DN3 accumulation, DN4 loss, reduced CD27 expression, and diminished DP cell output, we have strong evidence that *Csf1r*-expressing myeloid cells support thymocyte differentiation at the β-selection checkpoint. Thus, the thymic myeloid compartment contributes not only to tissue clearance and homeostasis but also to the microenvironmental conditions required for efficient early αβ T cell development.

Discussion

This study defines the mouse TM compartment as a developmentally dynamic network of phenotypically and transcriptionally specialized macrophages and connects the thymic myeloid niche to an early checkpoint in αβ T cell development. By integrating prospective surface-marker definition with single-cell transcriptomics, fate mapping, genetic perturbation, and organ culture, we identify two major TM populations with distinct functional programs and developmental contributions, demonstrate CCR2 dependence of the TIMD4- VCAM1 +population, and show that *Csf1r*-expressing myeloid cells support efficient DN3-to-DN4 progression.

The TIMD4 +VCAM1+population displayed a coherent efferocytic identity, including Mertk expression, enrichment of phagocytosis and endocytosis pathways, and detection of thymocyte-associated transcripts within a macrophage subcluster. Although these cells expressed *Spic*, preservation of total TMs in *Spic-/-* mice distinguishes maintenance of the thymic compartment from the SpiC-dependent program of splenic RPMs (***Kohyama et al., 2009***). In contrast, TIMD4-VCAM1+macrophages were enriched for antigen-presentation and interferon-response pathways, suggesting specialization for immune surveillance and interactions with developing thymocytes. The surface-marker correspondence between these transcriptional states and the cortical TIMD4+ and medullary/cortico-medullary CX3CR1+populations described by Zhou et al. provides a unified phenotypic and functional framework (***Zhou et al., 2022***).

The ontogeny experiments further reveal how this functional diversity is maintained. TIMD4+VCAM1+macrophages retained a substantial FLT3-independent embryonic/fetal contribution, whereas TIMD4-VCAM1+macrophages showed greater FLT3 history, representing a more dynamic population likely involved in immune surveillance (***Bain et al., 2014***; ***Davies et al., 2011***). The selective loss of TIMD4-VCAM1+macrophages and thymic monocytes in *Ccr2-/-* mice provides functional support for continuing recruitment from circulating precursors. These results confirm the broad dual-origin framework established by ***Zhou et al., 2022***, and extend it by identifying CCR2 as a requirement for maintenance of the TIMD4-VCAM1+arm of the network under steady-state conditions.

The functional studies reveal that the early αβ T cell program is sensitive to disruption of the thymic myeloid niche. The combination of DN3 accumulation, DN4 reduction, diminished CD27 expression, and reduced DP output localizes this requirement to progression at or near β-selection (***von Boehmer and Fehling, 1997***; ***Taghon et al., 2006***). Preservation of γδ T cells and TEC numbers argues against

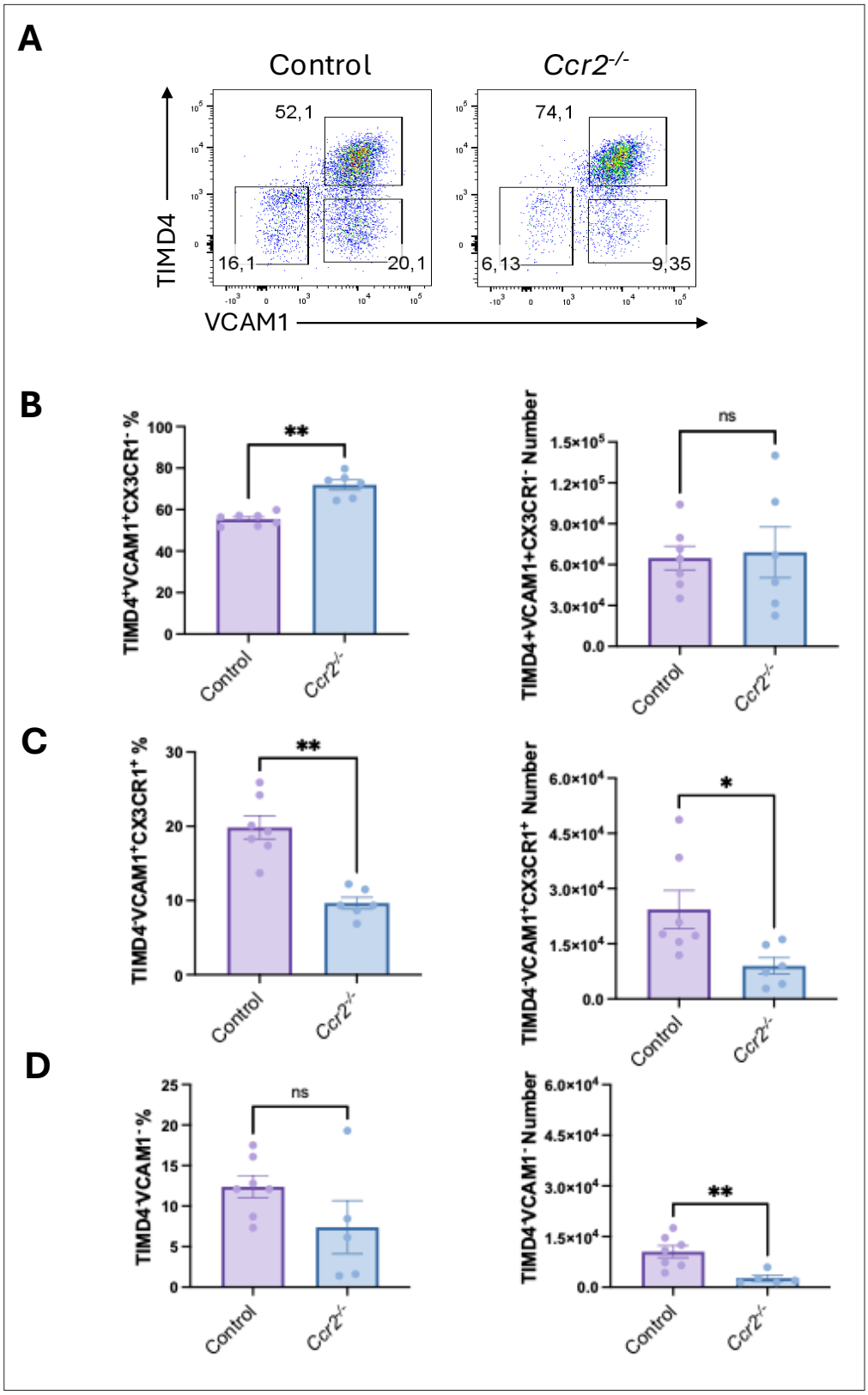


Figure 7. CCR2 dependence of TIMD4/VCAM1-defined thymic myeloid populations. (**A**) Representative TIMD4/VCAM1 profiles from *Ccr2-/-* and control mice. (**B–D**) Frequencies and absolute numbers of TIMD4+VCAM1+, TIMD4- VCAM1+, and TIMD4- VCAM1- populations. CX3CR1 phenotype is defined independently in ***Figure 2*** and is not displayed in this Figure. Data are mean ± SEM (n=6–7 per group from two independent experiments). Two-tailed Mann-Whitney test (*p≤0.05; **p≤0.01; ***p≤0.001).

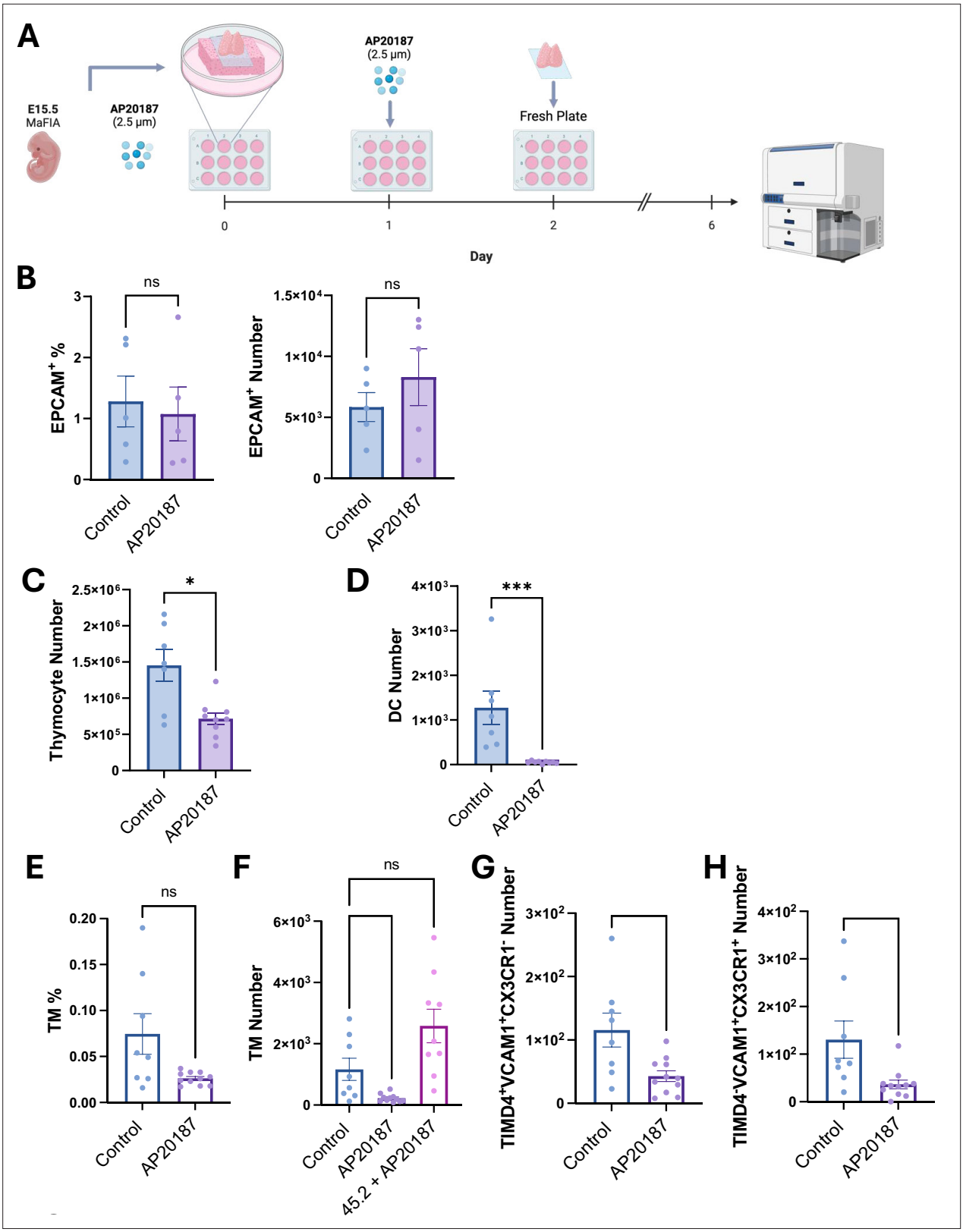


Figure 8. Efficient depletion of *Csf1r*-expressing myeloid cells in MaFIA fetal thymic organ culture. E15.5 MaFIA thymus lobes were treated with AP20187 at culture initiation and the following day, transferred to fresh FTOC media on day 2, and analyzed on day 6. (**A**) Experimental workflow. (**B**) EpCAM +CD45- thymic epithelial-cell frequencies and numbers. (**C**) Total thymocyte numbers. (**D**) CD45+CD11c+MHC-II^{high} DC numbers. (**E, F**) TM frequencies and absolute numbers in untreated and AP20187-treated MaFIA FTOCs and in AP20187-treated C57BL/6 J (CD45.2) control FTOCs. CD45.2

Figure 8 continued on next page

Figure 8 continued

denotes the congenic allele of the C57BL/6 J control. (**G, H**) Numbers of TIMD4+VCAM1+and TIMD4- VCAM1+TMs. The preservation of epithelial-cell and control-FTOC TM numbers, together with depletion of both MaFIA TM populations, demonstrates transgene-dependent perturbation of the *Csf1r*-expressing thymic myeloid compartment. Data are mean +/- SEM (n=8–11 per group from three independent experiments). Mann-Whitney or Kruskal-Wallis tests as indicated (*p ≤ 0.05; **p ≤ 0.01; ***p ≤ 0.001).

The online version of this article includes the following figure supplement(s) for figure 8:

Figure supplement 1. MaFIA transgene and reporter expression in thymic macrophages.

a uniform collapse of fetal thymic development and instead identifies a selective vulnerability of the αβ-lineage developmental pathway. These findings expand the established homeostatic role of thymic myeloid cells by showing that their presence is linked to efficient navigation of the first TCRβ rearrangement-dependent checkpoint.

Several complementary mechanisms could account for this myeloid-cell requirement. TIMD4 +macrophages are positioned and transcriptionally equipped to clear apoptotic thymocytes efficiently; their depletion could increase local cellular debris or alter the anti-inflammatory signals normally generated during efferocytosis, including TGF-β and IL-10 (***Kim et al., 2004***; ***Chung et al., 2006***; ***Huynh et al., 2002***). Myeloid cells may also provide survival, metabolic, or receptor-ligand signals that cooperate with pre-TCR and Notch pathways necessary for DN3-to-DN4 progression (***Duke-Cohan et al., 2023***; ***Li et al., 2021***; ***Mizsei et al., 2021***; ***Ciofani et al., 2006***; ***Ciofani et al., 2004***; ***Ciofani and Zúñiga-Pflücker, 2005***). The MaFIA mouse model depletes a *Csf1r*-expressing compartment that includes TMs, monocytes, and DCs, and our experiments did not directly assess *Csf1r*-transgene expression or AP20187-induced apoptosis in purified DN thymocytes. Consequently, the current data establish the requirement at the level of the *Csf1r*-expressing myeloid niche rather than assigning it to one macrophage subset or a single molecular mechanism. Although our depletion strategy also affected DCs, several lines of evidence implicate TMs as the primary mediators of this effect. The β-selection checkpoint occurs in the thymic cortex, a region densely populated by TMs, whereas DCs are largely restricted to the medulla and cortico-medullary junction (***Hadeiba et al., 2012***).This evidence-matched cellular resolution sharpens the developmental conclusion and provides a focused basis for future cell-restricted studies.

In conclusion, this study provides an integrated phenotypic, transcriptional, and developmental map of mouse TMs and demonstrates that the TIMD4- VCAM1 +population depends on CCR2-mediated precursor input. Most importantly, the organ culture experiments identify an intact *Csf1r*-expressing myeloid compartment as a requirement for efficient progression across the DN3-to-DN4 checkpoint. These findings place TM heterogeneity within a broader developmental framework and establish the thymic myeloid niche as an active component of early T cell development.

Materials and methods

Key resources table

Reagent type (species) or resource	Designation	Source or reference	Identifiers	Additional information
Strain, strain background (*Mus musculus*)	C57BL/6 J	The Jackson Laboratory	JAX:000664; RRID:IMSR_JAX:000664	Wild-type controls and source strain for adult and timed-pregnancy experiments
Genetic reagent (*M. musculus*)	MaFIA; Csf1r-EGFP/Fas-FKBP	The Jackson Laboratory	JAX:005070; RRID:IMSR_JAX:005070	Macrophage Fas-Induced Apoptosis model used for inducible depletion of Csf1r+myeloid cells
Genetic reagent (*M. musculus*)	MafB-mCherry-Cre	The Jackson Laboratory	JAX:029664; RRID:IMSR_JAX:029664	Reporter/Cre line used for thymic macrophage subset characterization
Genetic reagent (*M. musculus*)	Csf1r-EGFP	The Jackson Laboratory	JAX:018549; RRID:IMSR_JAX:018549	Reporter line used to detect Csf1r-expressing macrophages
Genetic reagent (*M. musculus*)	Spic−/−	The Jackson Laboratory	JAX: 013039; RRID:IMSR_JAX:013039	SpiC knockout mice; exact stock identifier not reported in manuscript

Continued on next page

Continued

Reagent type (species) or resource	Designation	Source or reference	Identifiers	Additional information
Genetic reagent (*M. musculus*)	Flt3-Cre×Rosa-mTmG	The Jackson Laboratory	Rosa-mTmG: JAX:007676; RRID:IMSR_JAX:007676	Fate-mapping mice; provided by Dr. Slava Epelman as stated in the manuscript
Genetic reagent (*M. musculus*)	Ccr2−/−	The Jackson Laboratory	JAX: 004999; RRID:IMSR_JAX:004999	Ccr2 knockout line used to backcross into fate mapping Flt3-Cre×Rosa mTmG mice, as stated in the manuscript
Genetic reagent (*M. musculus*)	Flt3-Cre×Rosa mTmG; Ccr2−/− background	PMID:24439267	Not commercially available	Fate-mapping mice in Ccr2 knockout background; provided by Dr. Slava Epelman as stated in the manuscript
Antibody	APC anti-mouse CD64/FcγRI (clone X54-5/7.1, mouse monoclonal)	BioLegend	Cat#:139305; RRID:AB_11219205; Cat#:139306; RRID:AB_11219391	Flow cytometry (1:200); manuscript reports clone/fluor/vendor but not purchased size
Antibody	BUV805 anti-mouse F4/80 (clone T45-2342, rat monoclonal)	BD Biosciences	Cat#:749282; RRID:AB_2873657	Flow cytometry (1:200)
Antibody	FITC anti-mouse MERTK/Mer (clone 2B10C42, rat monoclonal)	BioLegend	Cat#:151503; RRID:AB_2617034; Cat#:151504; RRID:AB_2617035	Flow cytometry (1:200); manuscript reports clone/fluor/vendor but not purchased size
Antibody	PE anti-mouse Tim-4 (clone RMT4-54, rat monoclonal)	BioLegend	Cat#:130005; RRID:AB_1227807; Cat#:130006; RRID:AB_2201843	Flow cytometry (1:200); manuscript reports clone/fluor/vendor but not purchased size
Antibody	PE/Cyanine7 anti-mouse CD106/VCAM1 (clone 429/MVCAM.A, rat monoclonal)	BioLegend	Cat#:105719; RRID:AB_2214047; Cat#:105720; RRID:AB_2214046	Flow cytometry (1:200); manuscript reports clone/fluor/vendor but not purchased size
Antibody	Brilliant Violet 605 anti-mouse CX3CR1 (clone SA011F11, mouse monoclonal)	BioLegend	Cat#:149027; RRID:AB_2565937	Flow cytometry (1:200)
Antibody	Brilliant Violet 785 anti-mouse CD192/CCR2 (clone SA203G11, rat monoclonal)	BioLegend	Cat#:150621; RRID:AB_2721565	Flow cytometry (1:200)
Antibody	APC/Cyanine7 anti-mouse/human CD11b (clone M1/70, rat monoclonal)	BioLegend	Cat#:101225; RRID:AB_830641; Cat#:101226; RRID:AB_830642	Flow cytometry (1:200); manuscript reports clone/fluor/vendor but not purchased size
Antibody	Brilliant Violet 711 anti-mouse Ly-6C (clone HK1.4, rat monoclonal)	BioLegend	Cat#:128037; RRID:AB_2562630	Flow cytometry (1:200)
Antibody	Alexa Fluor 700 anti-mouse I-A/I-E (clone M5/114.15.2, rat monoclonal)	BioLegend	Cat#:107621; RRID:AB_493726; Cat#:107622; RRID:AB_493727	Flow cytometry (1:200); manuscript reports clone/fluor/vendor but not purchased size
Antibody	BUV395 anti-mouse CD11c (clone N418, Armenian hamster monoclonal)	BD Biosciences	Cat#:744180; RRID:AB_2742045	Flow cytometry (1:200)
Antibody	BUV563 anti-mouse CD45 (clone 30-F11, rat monoclonal)	BD Biosciences	Cat#:565710; RRID:AB_2722550; Cat#:612924; RRID:AB_2870209	Flow cytometry (1:150); manuscript reports clone/fluor/vendor but not purchased size
Antibody	Purified anti-mouse CD16/32 Fc block (clone 93, rat monoclonal)	BioLegend	Cat#:101301; RRID:AB_312800; Cat#:101302; RRID:AB_312801	Flow cytometry/Fc block (1:100); manuscript reports clone/vendor but not purchased size
Antibody	PE/Cyanine7 anti-mouse CD3ε (clone 145–2 C11, Armenian hamster monoclonal)	BioLegend	Cat#:100319; Cat#:100320; RRID:AB_312685	Flow cytometry (1:200); manuscript reports clone/fluor/vendor but not purchased size

Continued on next page

Continued

Reagent type (species) or resource	Designation	Source or reference	Identifiers	Additional information
Antibody	Brilliant Violet 711 anti-mouse CD4 (clone RM4-5, rat monoclonal)	BioLegend	Cat#:100549; RRID:AB_11219396; Cat#:100550; RRID:AB_2562099; Cat#:100557; RRID:AB_2562607	Flow cytometry (1:200); manuscript reports clone/fluor/vendor but not purchased size
Antibody	BUV395 anti-mouse CD8a (clone 53–6.7, rat monoclonal)	BD Biosciences	Cat#:563786; RRID:AB_2732919	Flow cytometry (1:200)
Antibody	APC/Cyanine7 anti-mouse CD25 (clone PC61, rat monoclonal)	BioLegend	Cat#:102025; RRID:AB_830744; Cat#:102026; RRID:AB_830745	Flow cytometry (1:200); manuscript reports clone/fluor/vendor but not purchased size
Antibody	Brilliant Violet 785 anti-mouse/human CD44 (clone IM7, rat monoclonal)	BioLegend	Cat#:103041; RRID:AB_11218802; Cat#:103059; RRID:AB_2571953	Flow cytometry (1:200); manuscript reports clone/fluor/vendor but not purchased size
Antibody	Alexa Fluor 700 anti-mouse/human CD45R/B220 (clone RA3-6B2, rat monoclonal)	BioLegend	Cat#:103231; RRID:AB_493716; Cat#:103232	Flow cytometry (1:200); manuscript reports clone/fluor/vendor but not purchased size
Commercial assay or kit	Spleen Dissociation Kit	Miltenyi Biotec	Cat#:130-095-926; RRID:SCR_024888	Used for thymus dissociation prior to flow cytometry and sorting
Commercial assay or kit	Chromium Single Cell 3' Reagent Kit	10 x Genomics	Cat#:PN-1000691	Used for scRNA-seq library preparation; exact kit version not reported
Commercial assay or kit	anti-APC MicroBeads	Miltenyi Biotec	Cat#:130-090-855; RRID:AB_244367	Used for CD64 + cell enrichment prior to sorting
Commercial assay or kit	LS Columns	Miltenyi Biotec	Cat#:130-042-401	Used for positive selection of CD64 + cells
Chemical compound, drug	AP20187; B/B homodimerizer	Takara Bio	Cat#:635058	Used for MaFIA-mediated depletion in FTOC; vendor/catalog not reported in manuscript
Software, algorithm	FlowJo	BD/Tree Star	RRID:SCR_008520	Flow cytometry analysis
Software, algorithm	R (version 4.4.1)	R Project	RRID:SCR_001905	Statistical computing and scRNA-seq analysis
Software, algorithm	Seurat	Satija Lab / CRAN	RRID:SCR_007322	scRNA-seq processing, integration, clustering, SCTransform, FindMarkers
Software, algorithm	Harmony	***Korsunsky et al., 2019***	RRID:SCR_022206	Batch correction/data integration
Software, algorithm	Monocle3	Trapnell Lab	RRID:SCR_018685	Trajectory analysis / pseudotime inference
Software, algorithm	GraphPad Prism (version 10)	GraphPad	RRID:SCR_002798	Statistical analysis and graphing

Animals

Macrophage Fas-Induced Apoptosis (MaFIA), *Mafb*$^{mCherry\text{-}Cre}$, *Csf1r*^{EGFP}, *Spic*$^{-/-}$, and C57BL/6 J mice were purchased from the Jackson Laboratory. The *Flt3*^{Cre} × *Rosa26*^{mTmG} mice and *Flt3*^{Cre} × *Rosa26*^{mTmG} mice in the *Ccr2*$^{-/-}$ background were kindly provided by Dr. Slava Epelman (University Health Network, University of Toronto) (***Epelman et al., 2014***). All animals were bred and maintained in specific pathogen-free conditions at the Preclinical Research Centre of the Sunnybrook Research Institute (SRI). All animal procedures were approved by the Sunnybrook Health Sciences Centre Animal Care Committee (Toronto, Ontario, Canada).

Timed pregnancies and embryonic thymus analysis

Timed pregnancies were set up by housing male mice (8–24 weeks of age) in separate cages and mating them with female mice (8–24 weeks of age) overnight. The following morning, females were separated from the males, and successful matings were identified by the presence of a vaginal plug. The gestational age of the embryos was designated as embryonic day 0.5 (E0.5) on the day the plug was observed. Thymuses were harvested from embryos at E15 and E17, as well as from postnatal

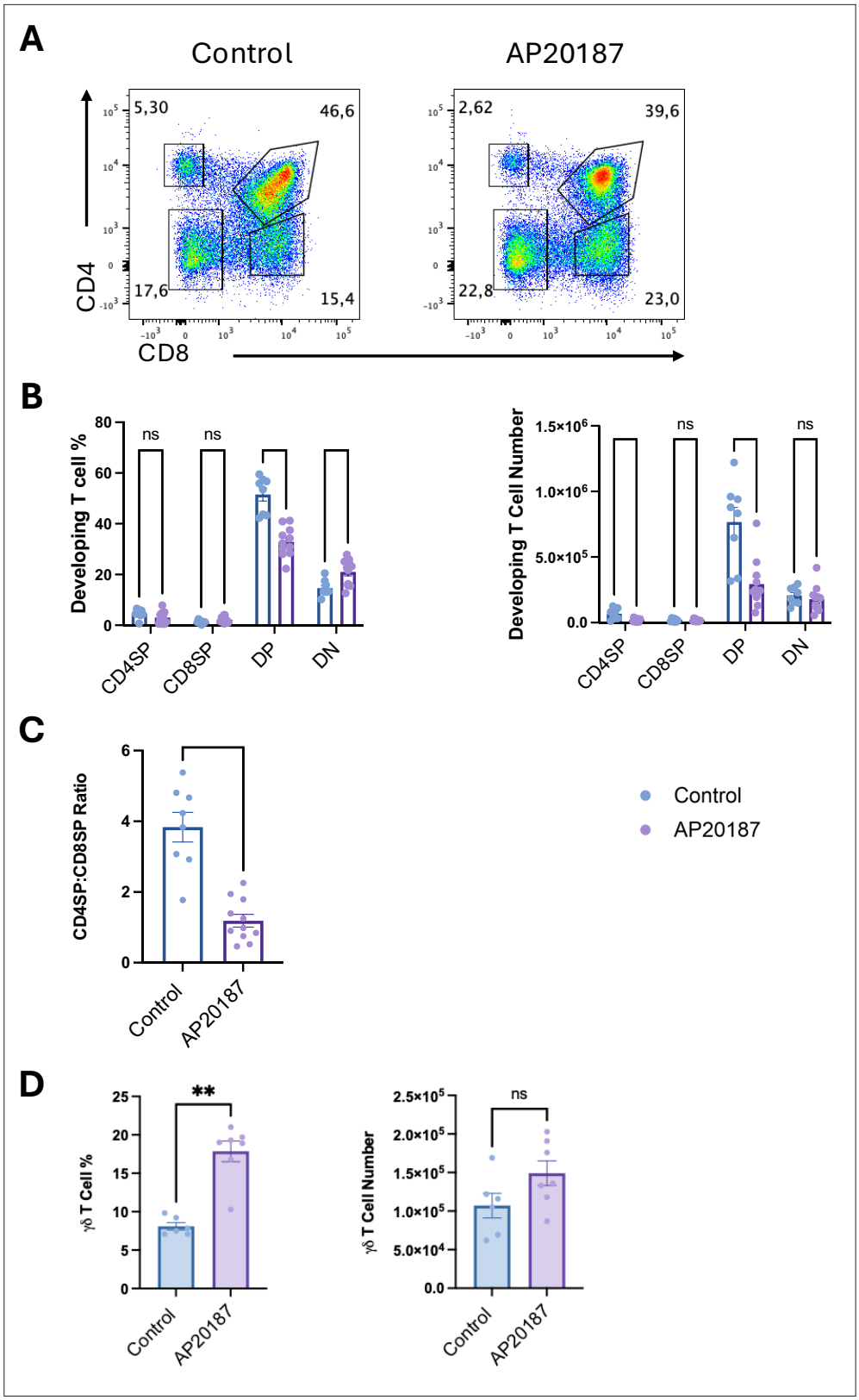


Figure 9. *Csf1r*-expressing myeloid cells support alpha-beta T cell development in FTOC. (**A**) Representative CD4/CD8 profiles. (**B**) Frequencies and absolute numbers of thymocyte populations in untreated and AP20187-treated MaFIA FTOCs. (**C**) CD3+CD4SP-to-CD3+CD8 SP ratio. (**D**) Frequencies and numbers of γδ T cells. Depletion reduced αβ-lineage DP thymocyte production while preserving γδ T cell output. Data are mean +/- SEM (n=8–

Figure 9 continued on next page

Figure 9 continued

11 per group from three independent experiments; γδ T cells, n=6–7 from two experiments). Mann-Whitney tests with Holm-Sidak correction (*p ≤ 0.05; **p ≤ 0.01; ***p ≤ 0.001).

mice at 1 day, 1 week, and 3 weeks of age, in addition to adult (6–8 weeks) mice. Following collection, thymuses were subjected to enzymatic digestion to dissociate the tissue into single-cell suspensions. The resulting cells were stained for flow cytometric analysis.

Intravenous CD45 staining

A CD45-Phycoerythrin (PE) antibody (30-F11; BioLegend) was diluted in PBS to a final concentration of 1.5 µg/150 µL. The antibody solution was administered via tail vein injection using a 1 mL insulin syringe. Three minutes after the injection, mice were euthanized, and thymuses were harvested. The collected tissue was then processed and stained for flow cytometric analysis.

Cell isolation from thymus

Thymocytes were harvested and subjected to enzymatic digestion using the Spleen Dissociation Kit (Miltenyi Biotec) and the gentleMACS Dissociator (Miltenyi Biotec) according to the manufacturer's instructions. The resulting cell suspensions were filtered through a 70 µm cell strainer to remove debris, resuspended in PBS, and kept on ice until further processing.

Flow cytometry

Single-cell suspensions (1×10^7 cells) were prepared from the thymus and stained in a 96-well conical bottom plate (Thermo Fisher Scientific). The staining cocktail included the fixable viability dye eFluor 450 (eBioscience), diluted 1:800 in PBS, anti-CD16/32 to block Fc receptors, and the desired fluorochrome-conjugated antibodies targeting macrophages and T cells (see ***Supplementary file 1, table 1 and 2*** for details). Cells were initially stained with eFluor 450 in PBS for 15 min on ice. After washing with fluorescence-activated cell sorting (FACS) buffer, anti-CD64, anti-CCR2, and anti-VCAM1 antibodies were added to the wells, and cells were stained for an additional 15 min on ice. To block non-specific binding, Fc-block antibody was added to the cells 15 min prior to the addition of the remaining antibody cocktail, which was incubated with the cells for 30 min on ice.

Following staining, cells were washed and resuspended in FACS buffer for flow cytometric acquisition using the FACSymphony A5 Cell Analyzer (BD Biosciences). Data were analyzed with FlowJo software (TreeStar). The complete list of antibodies and their corresponding clones is provided in ***Supplementary file 1, table 1 and 2***.

Cell sorting

Thymuses were harvested from 6-week-old C57BL/6 mice and subjected to enzymatic digestion using the Spleen Dissociation Kit (Miltenyi Biotec) and the gentleMACS Dissociator (Miltenyi Biotec) to generate single-cell suspensions. After cell isolation, cells were counted and stained with allophycocyanin (APC)-conjugated anti-mouse CD64 antibody in FACS buffer for 20 min on ice (see ***Supplementary file 1, table 1*** for antibody details). Following a wash with FACS buffer, cells were stained with anti-APC MicroBeads (Miltenyi Biotec) for 20 min on ice. The cells were then washed again with FACS buffer and loaded onto LS columns (Miltenyi Biotec) for positive selection of $CD64^+$ cells. After selection, the cells were washed and further stained with antibodies against F4/80, TIMD4, Ly6C, and CD45 for 30 min on ice (see ***Supplementary file 1, table 1*** for antibody details). The stained cells were sorted using the FACSAria Fusion Flow Cytometer (BD Biosciences). $CD64^+$ sorted cells were collected in 1.5 mL Eppendorf tubes containing 300 µL of FBS, counted, and resuspended in PBS supplemented with 0.04% BSA. Cells were then encapsulated, and library preparation was performed using the Chromium Single Cell 3' Reagent Kit (10 X Genomics). Gene expression libraries were sequenced on a NovaSeq 6000 platform (Illumina) at Azenta Life Sciences. In total, 3214 and 2815 cells were sequenced from two independent experiments.

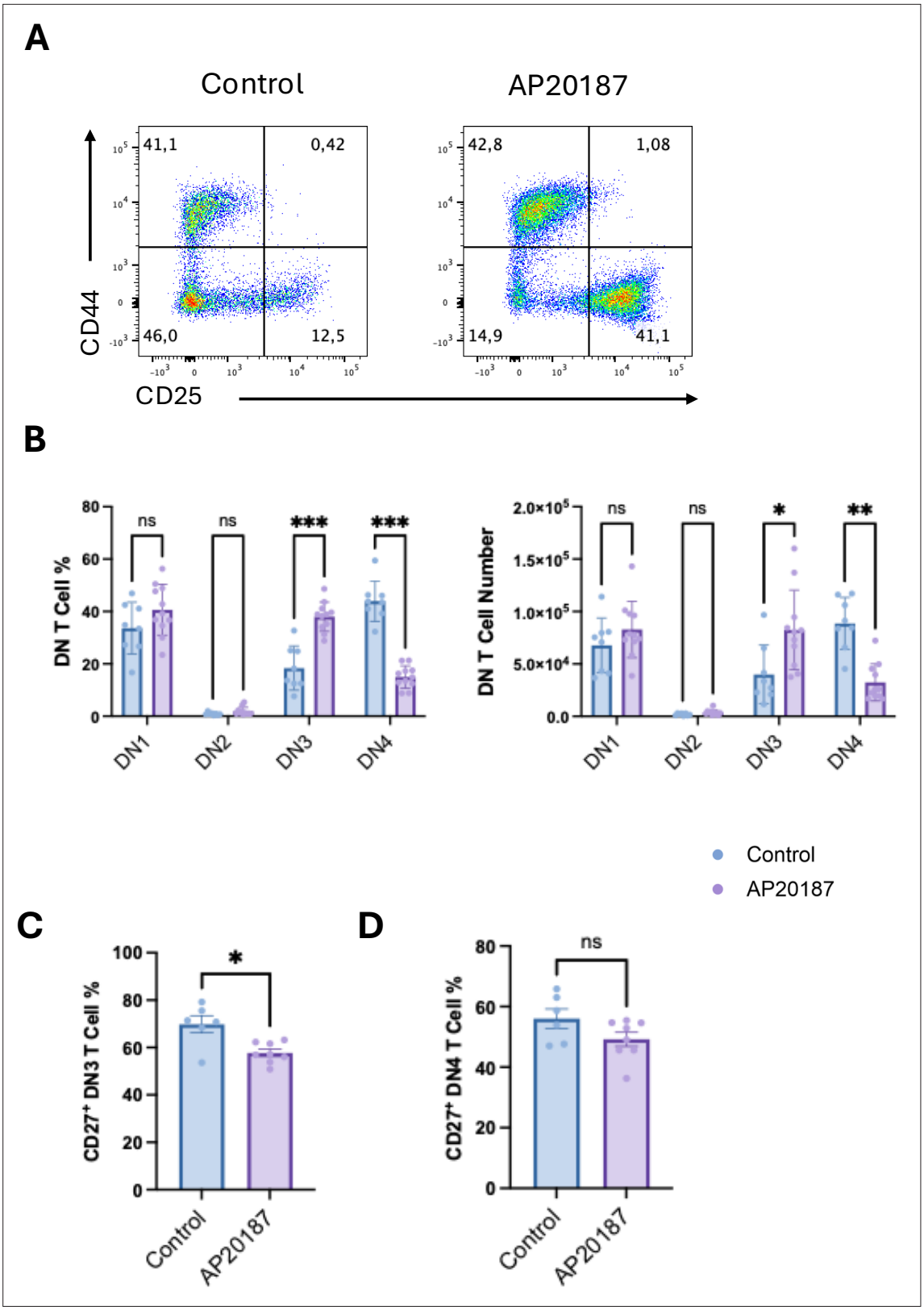


Figure 10. *Csf1r*-expressing myeloid cells support progression across the DN3-to-DN4 checkpoint. (**A**) Representative CD44/CD25 profiles of DN populations. (**B**) Frequencies and absolute numbers of DN subsets in untreated and AP20187-treated MaFIA FTOCs. (**C, D**) Quantified frequencies of CD27+DN3 and DN4 cells. The coordinated accumulation of DN3 cells, reduction of DN4 cells, and lower CD27 expression identify impaired progression at the β-selection transition. Data are mean +/- SEM (DN subsets, n=8–11 from three independent experiments; CD27, n=6–8 from two experiments). Mann-Whitney tests with Holm-Sidak correction (*p ≤ 0.05; **p ≤ 0.01; ***p ≤ 0.001).

Fetal thymus organ culture (FTOC) and TM depletion in MaFIA mice

Timed pregnancies were set up for MaFIA mice as described above. Fetal thymuses were harvested at E15.5 for FTOC. Briefly, culture wells were set up in a 12-well-plate 24 hr before FTOC. In each well, Whatman Nuclepore Track-Etched membrane (WHA110409; Sigma) was placed on top of SURGIFORM absorbable gelatin sponge (1974; Ethicon) in 1.5 mL of complete Dulbecco's Modified Eagle Medium (DMEM) (supplemented with 10% Fetal Bovine Serum, 2 mM L-glutamine, 100 U/mL penicillin, and 100 µg/mL streptomycin; ***Han and Zúñiga-Pflücker, 2021***; ***Nitta et al., 2013***). Three fetal thymuses were placed on top of the membrane for each well. B/B homodimerizer stock was diluted to 2.5 µM in complete DMEM and added to the thymus lobes at the time of culture setup and again on the following day. On day 2, the membrane with the thymus lobes was transferred to a fresh culture plate containing new gelatin sponge and complete DMEM. Cultures were maintained in a 37 °C incubator until day 6, at which point the thymic lobes were processed for flow cytometry analysis as described above.

Transcriptomic analysis

$CD64^+$ cells were isolated from the thymus of C57BL/6 J adult mice and processed for scRNA-seq as described below. Data from each scRNA-seq experiment underwent pre-processing as detailed below. Quality control filters were applied to remove cells with more than 12.5% mitochondrial gene expression, fewer than 500 reads, or more than 6000 reads, ensuring the retention of high-quality cells for analysis. Macrophages and monocytes were identified using a module scoring approach, and their respective cell barcodes were recorded. These barcodes were used for subsetting before merging the datasets from the two scRNA-seq experiments with published TM data from Dzhagalov's group. The merging was performed using Harmony to align the datasets and correct for batch effects. Following integration, cells were clustered, and module scores were assigned to all identified clusters. Non-relevant cell types, including B cells, T cells, and DCs, were excluded from subsequent analyses to focus on macrophages and monocytes.

Analysis of scRNA-Seq and data integration

All analyses were performed using R software version 4.4.1. Cells expressing fewer than 500 genes or more than 6000 genes were excluded from the dataset (GEO: GSE326594). Additionally, cells with greater than 12.5% mitochondrial gene content were removed to ensure data quality. The dimensionality of the dataset was assessed using an Elbow plot to determine the appropriate number of principal components. GO enrichment analysis of differentially expressed genes (DEGs) was conducted to identify overrepresented biological processes using the FindMarkers function from the Seurat package (***Satija et al., 2015***). The data were then integrated with previously published scRNA-seq datasets on TMs (GEO: GSE185460), as well as datasets from heart, liver, and lung macrophages (GEO: GSE188647), from the laboratories of Drs. Dzhagalov and Epelman, respectively. Batch correction across datasets was performed using the Harmony package (***Zhou et al., 2022***; ***Dick et al., 2022***; ***Korsunsky et al., 2019***). Following integration, the merged dataset was normalized using the SCTransform method to account for technical variation. For data visualization, Uniform Manifold Approximation and Projection (UMAP) was applied to reduce dimensionality and enable visualization of cellular clustering patterns.

Trajectory analysis using Monocle3

Trajectory analysis was performed using Monocle3 to examine transcriptional relationships among monocytes and TMs (***Trapnell et al., 2014***). Following SCTransform normalization and integration in Seurat, the expression matrix, cell metadata, and gene metadata were used to construct a Monocle3 CellDataSet. Principal component analysis and UMAP were used for dimensionality reduction, followed by re-clustering and graph learning. *Ly6c2+Ccr2+*monocytes were assigned as the root population based on their established precursor phenotype. Pseudotime therefore represents a model of transcriptional progression from a monocyte-like state and is interpreted together with, rather than independently of, the genetic fate-mapping and CCR2-dependence data.

Statistical analysis

Data are presented as the mean ± SEM. Univariate comparisons between two groups were performed using the Mann-Whitney U test. For analyses involving more than two groups, the normality of the data was assessed using the D'Agostino-Pearson test and/or inspection of Q-Q plots, while homoscedasticity (equal variance) was evaluated using the Brown-Forsythe test or by examining residual plots. Non-parametric comparisons across multiple groups were conducted using the Kruskal-Wallis test, followed by post-hoc pairwise comparisons of the mean ranks of each group with the mean rank of the control group. Multiple comparisons were adjusted using Dunn's test to control for type I error. For pairwise comparisons involving more than two groups, the Holm-Šídák method was applied to correct for multiple comparisons, reducing the likelihood of type I error. All statistical analyses were performed using GraphPad Prism version 10.

Additional information

Competing interests

Juan Carlos Zúñiga-Pflücker: Reviewing editor, eLife. The other authors declare that no competing interests exist.

Funding

Funder	Grant reference number	Author
Canadian Institutes of Health Research	FDN154332	Juan Carlos Zúñiga-Pflücker
Canadian Institutes of Health Research	PJT192050	Juan Carlos Zúñiga-Pflücker
Natural Sciences and Engineering Research Council of Canada	RGPIN-2024-05661	Juan Carlos Zúñiga-Pflücker
Canadian Institutes of Health Research	Postdoctoral Fellowship	Vinothkumar Rajan

The funders had no role in study design, data collection and interpretation, or the decision to submit the work for publication.

Author contributions

Helen Wang, Conceptualization, Data curation, Formal analysis, Investigation, Visualization, Methodology, Writing – original draft; Vinothkumar Rajan, Data curation, Formal analysis, Validation, Methodology; Anthony Wong, Resources, Validation, Methodology, Writing – review and editing; Slava Epelman, Resources, Methodology, Writing – review and editing; Juan Carlos Zúñiga-Pflücker, Conceptualization, Formal analysis, Supervision, Funding acquisition, Validation, Project administration, Writing – review and editing

Author ORCIDs

Juan Carlos Zúñiga-Pflücker https://orcid.org/0000-0003-2538-3178

Ethics

All animals were bred and maintained in specific pathogen-free conditions at the Preclinical Research Centre of the Sunnybrook Research Institute (SRI). All animal procedures were approved by the Sunnybrook Health Sciences Centre Animal Care Committee (Toronto, Ontario, Canada).

Peer review material

Version of Record:

Reviewer #1 (Public review): https://doi.org/10.7554/eLife.109219.3.sa1
Reviewer #2 (Public review): https://doi.org/10.7554/eLife.109219.3.sa2
Author response https://doi.org/10.7554/eLife.109219.3.sa3

Reviewed preprint v2

Reviewer #1 (Public review): https://doi.org/10.7554/eLife.109219.2.sa2
Reviewer #2 (Public review): https://doi.org/10.7554/eLife.109219.2.sa1
Author response: https://doi.org/10.7554/eLife.109219.2.sa0
eLife Assessment https://doi.org/10.7554/eLife.109219.2.sa3

Reviewed preprint v1
Reviewer #1 (Public review): https://doi.org/10.7554/eLife.109219.1.sa1
Reviewer #2 (Public review): https://doi.org/10.7554/eLife.109219.1.sa0
eLife Assessment https://doi.org/10.7554/eLife.109219.1.sa2

Additional files

Supplementary files

MDAR checklist

Supplementary file 1. Supplemental tables.

Data availability

Single cell RNAseq datasets have been deposited to the Gene Expression Omnibus (GEO) repository, accession number GSE326594.

The following dataset was generated:

Author(s)	Year	Dataset title	Dataset URL	Database and Identifier
Wang H, Zuniga-Pflucker JC	2026	Uncovering the Heterogeneity and Ontogeny of Mouse Thymic Macrophages Reveals an Unexpected Early Checkpoint Role	https://www.ncbi.nlm.nih.gov/geo/query/acc.cgi?acc=GSE326594	NCBI Gene Expression Omnibus, GSE326594

The following previously published datasets were used:

Author(s)	Year	Dataset title	Dataset URL	Database and Identifier
Hamidzada H, Epelman S	2022	Three tissue resident macrophage subsets co-exist across organs with conserved origins and lifecycles	https://www.ncbi.nlm.nih.gov/geo/query/acc.cgi?acc=GSE188647	NCBI Gene Expression Omnibus, GSE188647
Zhou T, Dzhagalov IL	2021	Single-cell RNA-sequencing of thymic myeloid cells from Csf1rgfp/gfp (MaFIA) and Cd11cyfp/yfp mice	https://www.ncbi.nlm.nih.gov/geo/query/acc.cgi?acc=GSE185460	NCBI Gene Expression Omnibus, GSE185460

References

Bain CC, Bravo-Blas A, Scott CL, Perdiguero EG, Geissmann F, Henri S, Malissen B, Osborne LC, Artis D, Mowat AM. 2014. Constant replenishment from circulating monocytes maintains the macrophage pool in the intestine of adult mice. *Nature Immunology* **15**:929–937. DOI: https://doi.org/10.1038/ni.2967, PMID: 25151491

Baratin M, Simon L, Jorquera A, Ghigo C, Dembele D, Nowak J, Gentek R, Wienert S, Klauschen F, Malissen B, Dalod M, Bajénoff M. 2017. T cell zone resident macrophages silently dispose of apoptotic cells in the lymph node. *Immunity* **47**:349–362. DOI: https://doi.org/10.1016/j.immuni.2017.07.019, PMID: 28801233

Benz C, Martins VC, Radtke F, Bleul CC. 2008. The stream of precursors that colonizes the thymus proceeds selectively through the early T lineage precursor stage of T cell development. *The Journal of Experimental Medicine* **205**:1187–1199. DOI: https://doi.org/10.1084/jem.20072168, PMID: 18458114

Burnett SH, Kershen EJ, Zhang J, Zeng L, Straley SC, Kaplan AM, Cohen DA. 2004. Conditional macrophage ablation in transgenic mice expressing a Fas-based suicide gene. *Journal of Leukocyte Biology* **75**:612–623. DOI: https://doi.org/10.1189/jlb.0903442, PMID: 14726498

Chung EY, Kim SJ, Ma XJ. 2006. Regulation of cytokine production during phagocytosis of apoptotic cells. *Cell Research* **16**:154–161. DOI: https://doi.org/10.1038/sj.cr.7310021, PMID: 16474428
Ciofani M, Schmitt TM, Ciofani A, Michie AM, Cuburu N, Aublin A, Maryanski JL, Zúñiga-Pflücker JC. 2004. Obligatory role for cooperative signaling by pre-TCR and Notch during thymocyte differentiation. *Journal of Immunology* **172**:5230–5239. DOI: https://doi.org/10.4049/jimmunol.172.9.5230, PMID: 15100261
Ciofani M, Zúñiga-Pflücker JC. 2005. Notch promotes survival of pre-T cells at the beta-selection checkpoint by regulating cellular metabolism. *Nature Immunology* **6**:881–888. DOI: https://doi.org/10.1038/ni1234, PMID: 16056227
Ciofani M, Knowles GC, Wiest DL, von Boehmer H, Zúñiga-Pflücker JC. 2006. Stage-specific and differential notch dependency at the alphabeta and gammadelta T lineage bifurcation. *Immunity* **25**:105–116. DOI: https://doi.org/10.1016/j.immuni.2006.05.010, PMID: 16814577
Ciofani M, Zúñiga-Pflücker JC. 2010. Determining γδ versus αß T cell development. *Nature Reviews. Immunology* **10**:657–663. DOI: https://doi.org/10.1038/nri2820, PMID: 20725107
Das DK, Mallis RJ, Duke-Cohan JS, Hussey RE, Tetteh PW, Hilton M, Wagner G, Lang MJ, Reinherz EL. 2016. Pre-T Cell Receptors (Pre-TCRs) Leverage Vβ Complementarity Determining Regions (CDRs) and hydrophobic patch in mechanosensing thymic self-ligands. *The Journal of Biological Chemistry* **291**:25292–25305. DOI: https://doi.org/10.1074/jbc.M116.752865, PMID: 27707880
Davies LC, Rosas M, Smith PJ, Fraser DJ, Jones SA, Taylor PR. 2011. A quantifiable proliferative burst of tissue macrophages restores homeostatic macrophage populations after acute inflammation. *European Journal of Immunology* **41**:2155–2164. DOI: https://doi.org/10.1002/eji.201141817, PMID: 21710478
Dick SA, Wong A, Hamidzada H, Nejat S, Nechanitzky R, Vohra S, Mueller B, Zaman R, Kantores C, Aronoff L, Momen A, Nechanitzky D, Li WY, Ramachandran P, Crome SQ, Becher B, Cybulsky MI, Billia F, Keshavjee S, Mital S, et al. 2022. Three tissue resident macrophage subsets coexist across organs with conserved origins and life cycles. *Science Immunology* **7**:eabf7777. DOI: https://doi.org/10.1126/sciimmunol.abf7777, PMID: 34995099
Duke-Cohan JS, Akitsu A, Mallis RJ, Messier CM, Lizotte PH, Aster JC, Hwang W, Lang MJ, Reinherz EL. 2023. Pre-T cell receptor self-MHC sampling restricts thymocyte dedifferentiation. *Nature* **613**:565–574. DOI: https://doi.org/10.1038/s41586-022-05555-7, PMID: 36410718
Epelman S, Lavine KJ, Beaudin AE, Sojka DK, Carrero JA, Calderon B, Brija T, Gautier EL, Ivanov S, Satpathy AT, Schilling JD, Schwendener R, Sergin I, Razani B, Forsberg EC, Yokoyama WM, Unanue ER, Colonna M, Randolph GJ, Mann DL. 2014. Embryonic and adult-derived resident cardiac macrophages are maintained through distinct mechanisms at steady state and during inflammation. *Immunity* **40**:91–104. DOI: https://doi.org/10.1016/j.immuni.2013.11.019, PMID: 24439267
Falk I, Nerz G, Haidl I, Krotkova A, Eichmann K. 2001. Immature thymocytes that fail to express TCRbeta and/or TCRgamma delta proteins die by apoptotic cell death in the CD44(-)CD25(-) (DN4) subset. *European Journal of Immunology* **31**:3308–3317. DOI: https://doi.org/10.1002/1521-4141(200111)31:11<3308::aid-immu3308>3.0.co;2-5, PMID: 11745348
Foss DL, Donskoy E, Goldschneider I. 2001. The importation of hematogenous precursors by the thymus is a gated phenomenon in normal adult mice. *The Journal of Experimental Medicine* **193**:365–374. DOI: https://doi.org/10.1084/jem.193.3.365, PMID: 11157056
Goldschneider I, Komschlies KL, Greiner DL. 1986. Studies of thymocytopoiesis in rats and mice. I. Kinetics of appearance of thymocytes using a direct intrathymic adoptive transfer assay for thymocyte precursors. *The Journal of Experimental Medicine* **163**:1–17. DOI: https://doi.org/10.1084/jem.163.1.1
Gotter J, Brors B, Hergenhahn M, Kyewski B. 2004. Medullary epithelial cells of the human thymus express a highly diverse selection of tissue-specific genes colocalized in chromosomal clusters. *The Journal of Experimental Medicine* **199**:155–166. DOI: https://doi.org/10.1084/jem.20031677, PMID: 14734521
Hadeiba H, Lahl K, Edalati A, Oderup C, Habtezion A, Pachynski R, Nguyen L, Ghodsi A, Adler S, Butcher EC. 2012. Plasmacytoid dendritic cells transport peripheral antigens to the thymus to promote central tolerance. *Immunity* **36**:438–450. DOI: https://doi.org/10.1016/j.immuni.2012.01.017, PMID: 22444632
Han J, Zúñiga-Pflücker JC. 2021. High-oxygen submersion fetal thymus organ cultures enable FOXN1-dependent and -independent support of T lymphopoiesis. *Frontiers in Immunology* **12**:652665. DOI: https://doi.org/10.3389/fimmu.2021.652665, PMID: 33859647
Hanna RN, Carlin LM, Hubbeling HG, Nackiewicz D, Green AM, Punt JA, Geissmann F, Hedrick CC. 2011. The transcription factor NR4A1 (Nur77) controls bone marrow differentiation and the survival of Ly6C- monocytes. *Nature Immunology* **12**:778–785. DOI: https://doi.org/10.1038/ni.2063, PMID: 21725321
Huynh MLN, Fadok VA, Henson PM. 2002. Phosphatidylserine-dependent ingestion of apoptotic cells promotes TGF-beta1 secretion and the resolution of inflammation. *The Journal of Clinical Investigation* **109**:41–50. DOI: https://doi.org/10.1172/JCI11638, PMID: 11781349
Italiani P, Boraschi D. 2014. From monocytes to M1/M2 macrophages: phenotypical vs. functional differentiation. *Frontiers in Immunology* **5**:514. DOI: https://doi.org/10.3389/fimmu.2014.00514, PMID: 25368618
James KD, Jenkinson WE, Anderson G. 2021. Non-epithelial stromal cells in thymus development and function. *Frontiers in Immunology* **12**:634367. DOI: https://doi.org/10.3389/fimmu.2021.634367, PMID: 33717173
Janeway CA, Travers P, Walport M, Shlomchik MJ. 2001. T-cell receptor gene rearrangement. In: Janeway CA (Ed). *Immunobiology: The Immune System in Health and Disease*. Garland Science. p. 137–141.
Jenkinson EJ, Anderson G. 1994. Fetal thymic organ cultures. *Current Opinion in Immunology* **6**:293–297. DOI: https://doi.org/10.1016/0952-7915(94)90104-x, PMID: 8011212

Kim S, Elkon KB, Ma X. 2004. Transcriptional suppression of interleukin-12 gene expression following phagocytosis of apoptotic cells. *Immunity* **21**:643–653. DOI: https://doi.org/10.1016/j.immuni.2004.09.009, PMID: 15539151

Klein L, Kyewski B, Allen PM, Hogquist KA. 2014. Positive and negative selection of the T cell repertoire: what thymocytes see (and don't see). *Nature Reviews. Immunology* **14**:377–391. DOI: https://doi.org/10.1038/nri3667, PMID: 24830344

Klein L, Petrozziello E. 2025. Antigen presentation for central tolerance induction. *Nature Reviews. Immunology* **25**:57–72. DOI: https://doi.org/10.1038/s41577-024-01076-8, PMID: 39294277

Kohyama M, Ise W, Edelson BT, Wilker PR, Hildner K, Mejia C, Frazier WA, Murphy TL, Murphy KM. 2009. Role for Spi-C in the development of red pulp macrophages and splenic iron homeostasis. *Nature* **457**:318–321. DOI: https://doi.org/10.1038/nature07472, PMID: 19037245

Korsunsky I, Millard N, Fan J, Slowikowski K, Zhang F, Wei K, Baglaenko Y, Brenner M, Loh P-R, Raychaudhuri S. 2019. Fast, sensitive and accurate integration of single-cell data with Harmony. *Nature Methods* **16**:1289–1296. DOI: https://doi.org/10.1038/s41592-019-0619-0, PMID: 31740819

Li X, Mizsei R, Tan K, Mallis RJ, Duke-Cohan JS, Akitsu A, Tetteh PW, Dubey A, Hwang W, Wagner G, Lang MJ, Arthanari H, Wang J-H, Reinherz EL. 2021. Pre-T cell receptors topologically sample self-ligands during thymocyte β-selection. *Science* **371**:181–185. DOI: https://doi.org/10.1126/science.abe0918, PMID: 33335016

Michie AM, Zúñiga-Pflücker JC. 2002. Regulation of thymocyte differentiation: pre-TCR signals and beta-selection. *Seminars in Immunology* **14**:311–323. DOI: https://doi.org/10.1016/s1044-5323(02)00064-7, PMID: 12220932

Miller JFAP. 2011. The golden anniversary of the thymus. *Nature Reviews. Immunology* **11**:489–495. DOI: https://doi.org/10.1038/nri2993, PMID: 21617694

Mizsei R, Li X, Chen W-N, Szabo M, Wang J-H, Wagner G, Reinherz EL, Mallis RJ. 2021. A general chemical crosslinking strategy for structural analyses of weakly interacting proteins applied to preTCR-pMHC complexes. *The Journal of Biological Chemistry* **296**:100255. DOI: https://doi.org/10.1016/j.jbc.2021.100255, PMID: 33837736

Moran AE, Hogquist KA. 2012. T-cell receptor affinity in thymic development. *Immunology* **135**:261–267. DOI: https://doi.org/10.1111/j.1365-2567.2011.03547.x, PMID: 22182461

Murata S, Takahama Y, Tanaka K. 2008. Thymoproteasome: probable role in generating positively selecting peptides. *Current Opinion in Immunology* **20**:192–196. DOI: https://doi.org/10.1016/j.coi.2008.03.002, PMID: 18403190

Nitta T, Ohigashi I, Takahama Y. 2013. The development of t lymphocytes in fetal thymus organ culture. In: Helgason CD, Miller CL (Eds). *Basic Cell Culture Protocols*. Humana Press. p. 85–102. DOI: https://doi.org/10.1007/978-1-62703-128-8_6

Palmer E. 2003. Negative selection--clearing out the bad apples from the T-cell repertoire. *Nature Reviews. Immunology* **3**:383–391. DOI: https://doi.org/10.1038/nri1085, PMID: 12766760

Petrie HT, Zúñiga-Pflücker JC. 2007. Zoned out: functional mapping of stromal signaling microenvironments in the thymus. *Annual Review of Immunology* **25**:649–679. DOI: https://doi.org/10.1146/annurev.immunol.23.021704.115715, PMID: 17291187

Proietto AI, van Dommelen S, Zhou P, Rizzitelli A, D'Amico A, Steptoe RJ, Naik SH, Lahoud MH, Liu Y, Zheng P, Shortman K, Wu L. 2008. Dendritic cells in the thymus contribute to T-regulatory cell induction. *PNAS* **105**:19869–19874. DOI: https://doi.org/10.1073/pnas.0810268105, PMID: 19073916

Rothenberg EV, Moore JE, Yui MA. 2008. Launching the T-cell-lineage developmental programme. *Nature Reviews. Immunology* **8**:9–21. DOI: https://doi.org/10.1038/nri2232, PMID: 18097446

Satija R, Farrell JA, Gennert D, Schier AF, Regev A. 2015. Spatial reconstruction of single-cell gene expression data. *Nature Biotechnology* **33**:495–502. DOI: https://doi.org/10.1038/nbt.3192, PMID: 25867923

Shah DK, Zúñiga-Pflücker JC. 2014. An overview of the intrathymic intricacies of T cell development. *Journal of Immunology* **192**:4017–4023. DOI: https://doi.org/10.4049/jimmunol.1302259, PMID: 24748636

Taghon T, Yui MA, Pant R, Diamond RA, Rothenberg EV. 2006. Developmental and molecular characterization of emerging beta- and gammadelta-selected pre-T cells in the adult mouse thymus. *Immunity* **24**:53–64. DOI: https://doi.org/10.1016/j.immuni.2005.11.012, PMID: 16413923

Thorp E, Cui D, Schrijvers DM, Kuriakose G, Tabas I. 2008. Mertk receptor mutation reduces efferocytosis efficiency and promotes apoptotic cell accumulation and plaque necrosis in atherosclerotic lesions of apoe-/- mice. *Arteriosclerosis, Thrombosis, and Vascular Biology* **28**:1421–1428. DOI: https://doi.org/10.1161/ATVBAHA.108.167197, PMID: 18451332

Trapnell C, Cacchiarelli D, Grimsby J, Pokharel P, Li S, Morse M, Lennon NJ, Livak KJ, Mikkelsen TS, Rinn JL. 2014. The dynamics and regulators of cell fate decisions are revealed by pseudotemporal ordering of single cells. *Nature Biotechnology* **32**:381–386. DOI: https://doi.org/10.1038/nbt.2859, PMID: 24658644

von Boehmer H, Fehling HJ. 1997. Structure and function of the pre-T cell receptor. *Annual Review of Immunology* **15**:433–452. DOI: https://doi.org/10.1146/annurev.immunol.15.1.433, PMID: 9143695

Wang H, Zúñiga-Pflücker JC. 2022. Thymic microenvironment: interactions between innate immune cells and developing thymocytes. *Frontiers in Immunology* **13**:885280. DOI: https://doi.org/10.3389/fimmu.2022.885280

Zhou T-A, Hsu H-P, Tu Y-H, Cheng H-K, Lin C-Y, Chen N-J, Tsai J-W, Robey EA, Huang H-C, Hsu C-L, Dzhagalov IL. 2022. Thymic macrophages consist of two populations with distinct localization and origin. *eLife* **11**:e75148. DOI: https://doi.org/10.7554/eLife.75148, PMID: 36449334